JOURNAL OF NEUROTRAUMA 33:439–459 (March 1, 2016)
Mary Ann Liebert, Inc.
DOI: 10.1089/neu.2015.3956

Original Articles

A Unilateral Cervical Spinal Cord Contusion Injury Model in Non-Human Primates (*Macaca mulatta*)

Ernesto A. Salegio,[1] Jacqueline C. Bresnahan,[1] Carolyn J. Sparrey,[2] William Camisa,[3] Jason Fischer,[3] Jeremi Leasure,[3] Jennifer Buckley,[4] Yvette S. Nout-Lomas,[5] Ephron S. Rosenzweig,[6] Rod Moseanko,[7] Sarah Strand,[7] Stephanie Hawbecker,[7] Marie-Josee Lemoy,[7] Jenny Haefeli,[1] Xiaokui Ma,[1] Jessica L. Nielson,[1] V.R. Edgerton,[8] Adam R. Ferguson,[1] Mark H. Tuszynski,[6] and Michael S. Beattie[1]

Abstract

The development of a non-human primate (NHP) model of spinal cord injury (SCI) based on mechanical and computational modeling is described. We scaled up from a rodent model to a larger primate model using a highly controllable, friction-free, electronically-driven actuator to generate unilateral C6-C7 spinal cord injuries. Graded contusion lesions with varying degrees of functional recovery, depending upon pre-set impact parameters, were produced in nine NHPs. Protocols and pre-operative magnetic resonance imaging (MRI) were used to optimize the predictability of outcomes by matching impact protocols to the size of each animal's spinal canal, cord, and cerebrospinal fluid space. Post-operative MRI confirmed lesion placement and provided information on lesion volume and spread for comparison with histological measures. We evaluated the relationships between impact parameters, lesion measures, and behavioral outcomes, and confirmed that these relationships were consistent with our previous studies in the rat. In addition to providing multiple univariate outcome measures, we also developed an integrated outcome metric describing the multivariate cervical SCI syndrome. Impacts at the higher ranges of peak force produced highly lateralized and enduring deficits in multiple measures of forelimb and hand function, while lower energy impacts produced early weakness followed by substantial recovery but enduring deficits in fine digital control (e.g., pincer grasp). This model provides a clinically relevant system in which to evaluate the safety and, potentially, the efficacy of candidate translational therapies.

Key words: biomechanics of injury; contusion; functional recovery; primate; spinal cord injury

Introduction

Pre-clinical modeling of human spinal cord injury (SCI) has advanced to the point where a variety of well-characterized models of thoracic SCI are available in rodents and to a limited extent, large animals. Recently, more attention has been placed on cervical models of SCI, and several animal models are available.[1–7] However, there continues to be substantial challenges in translating laboratory success in rodent models of SCI to beneficial clinical outcomes.[8] As more therapeutic interventions near readiness for translation into human clinical trials, the use of large animal models, and non-human primates (NHPs) in particular, have been re-examined.[9,10]

The NHP spinal cord and central nervous system (CNS) more closely resemble humans than those of either rodent or porcine species, particularly when considering cervical injuries and forelimb/hand function. Previous studies using an NHP cervical spinal cord hemisection model identified important differences between rats and NHPs in corticospinal tract (CST) function and plasticity after injury.[11] Further, the macaque hemisection model was

[1]Department of Neurological Surgery, Brain and Spinal Injury Center, University of California at San Francisco, San Francisco, California.
[2]School of Engineering Science, Simon Fraser University, Surrey, British Columbia, Canada.
[3]Taylor Collaboration, St. Mary's Medical Center, San Francisco, California.
[4]Department of Mechanical Engineering, University of Delaware, Newark, Delaware.
[5]College of Veterinary Medicine and Biomedical Sciences, Colorado State University, Fort Collins, Colorado.
[6]Department of Neurosciences, University of California at San Diego, San Diego, California; Veterans Administration Medical Center, La Jolla, California.
[7]California National Primate Research Center, University of California at Davis, Davis, California.
[8]Departments of Physiological Science and Neurology, University of California at Los Angeles, Los Angeles, California.

developed to characterize recovery of function on a range of forelimb and locomotor tasks, and has provided new insights into recovery of function after SCI in primates.[12,13] Because most human SCIs are contusive or compressive in nature and occur with greatest frequency at the cervical level, we attempted to develop a model of unilateral contusion injury to more closely model the human injury without imposing severe functional deficits.

Based on our prior studies in the rat,[7,14–16] we planned to generate a unilateral contusion lesion at the C6-C7 spinal level that would result in prolonged forelimb deficits. We predicted that the extent and duration of behavioral deficit would vary as a function of lesion severity. Further, we aimed to develop a model that would allow evaluation of both potentially positive and negative effects of therapeutic interventions on partial cord injuries, like those suffered by many human SCI patients, and to provide a sensitive translational platform.

We used a pre-planning approach based on engineering considerations from prior rat injuries and scaled up using computational and surrogate cord modeling approaches.[17] We now report the design of the primate contusion device, the parameters of injury, sustainability of functional deficits as a function of varying lesion severities, and a multivariate syndromic analysis of the resulting dataset.[14,18] The ability to pre-set the injury level and predict outcomes from the resultant biomechanical parameters provides a potential means of efficiently testing candidate therapies in a NHP model that more closely approximates the human condition.

Methods

Subjects

Nine adult male NHPs *(Macaca mulatta)* were subjects of this study (Table 1). All housing and procedures were conducted in accordance with the National Institutes of Health (NIH) Guide for the Care and Use of Laboratory Animals, and were approved by The Institutional Animal Care and Use Committee at the University of California at Davis. The animal care and use program at the University of California at Davis is Association for Assessment and Accreditation of Laboratory Animal Care International accredited.

Impactor device and surrogate testing

Actuator. The TestBench™ system manufactured with a friction-free actuator design was developed by Bose® ElectroForce linear motor technology (Model 200N LM1; Bose Corporation, Eden Praire, MN). This system operates using Wintest® 7.0 closed loop control software, with powerful capabilities for real-time data acquisition and custom waveform generation. A structural support was custom-built to suspend the weight of the actuator (approximately 7.3 kg) over the surgical site, and was secured to a heavy-duty stereotaxic frame (Model 1504; David Kopf Instruments, Tujunga, CA,) on a spinal unit (Model 1780; David Kopf Instruments Tujunga CA; Fig. 1A, 1C). The support structure allowed positioning of the actuator in three dimensions. The impounder rod was fitted with a 15-mm long and 4-mm wide lucite tip (Fig. 1A inset and 1B), and two lasers adjacent to the impactor rod provided crosshairs for positioning the impounder on the exposed dura.

Impactor set-up. Mechanical parameters for the impacts were set with a 0.2 sec delay (dwell waveform) prior to initiating the downward excursion for an impact at a speed of 1 m/sec until reaching a specified vertical displacement (2.0-4.0 mm; ramp waveform), followed by a dwell time of 0.02 sec (dwell waveform) and fast retraction of the impounder at 1 m/sec to a height well above the zero start point (8 mm). An example is shown in Figure 1F; the green line indicates the pre-set waveform. Impact parameters were adjusted with each successive test subject (Table 2).

Surrogate testing. A silicone polymer surrogate spinal cord model (ellipsoid diameter a = 4.8 mm and diameter b = 8.9 mm) was manufactured to match the size and compressive properties of the spinal cord. To mimic the properties of the dura, cerebrospinal fluid (CSF), and vertebral canal, the surrogate cord was enclosed in a water-filled polyethylene plastic flat tubing and was placed in a metal trough (approximately the size of the vertebral canal) embedded in a Styrofoam block for stability. This surrogate model allowed for initial development of the force reading protocol to identify the dura, cord surface, and entrapment of the cord against the canal. It also allowed for the calibration, tuning, and testing of the impact protocol prior to each surgery. Thus, accurate and consistent force and displacement readouts prior to the actual *in vivo* impact were confirmed.[17]

Surgical procedures

Unilateral spinal cord contusion injury. The animals were sedated with ketamine (10 mg/kg IM; Mylan Institutional LLC, Rockford, IL) and atropine (0.05 mg/kg IM; Baxter HealthCare Corp., Deerfield, IL), intubated, and maintained at a surgical plane of anesthesia using isoflurane (1.5-2.0%; Piramal Critical Care Inc., Bethlehem, PA) and constant rate infusion of fentanyl citrate (7-10 μg/kg/h intravenously; Hospira Inc., Lake Forest, IL). The surgical site was prepared using standard aseptic techniques. The animal was place in a standard stereotaxic instrument (Model 1780; David Kopf Instruments). During surgery, body temperature, heart rate, respiration rate, and indirect blood pressure were closely

Table 1. Summary of Study

	Subject #1	*Subject #2*	*Subject #3*	*Subject #4*	*Subject #5*	*Subject #6*	*Subject #7*	*Subject #8*	*Subject #9*
Age (years/months)	7/11	7/1	7/3	6/5	7/0	6/7	11/11	7/2	9/6
Weight (kg)	8.8	10.9	13.2	9.3	14.7	10.8	11.0	11.9	15.2
Survival (weeks)	3	3	11	8	20	21	14	20	19
E-Cage	Yes	Yes	Yes	Yes	Yes	Yes	Yes	Yes	Yes
von Frey	No	No	No	No	Yes	Yes	Yes	Yes	No
Chair tasks*	No	No	No	No	Yes	Yes	Yes	Yes	No
EMG	No	No	No	No	No	No	Yes	No	No
Treadmill	No	No	No	No	No	No	Yes**	No	No
MRI	No	No	No	No	1.5T	1.5T	No	1.5T	3T
CST Tracing	No	No	No	No	Yes	Yes	No	Yes	No

*Chair tasks include platform, grape on the stick, handle pull, and Brinkman board.

**Subject #7 was the only animal implanted with electrodes for EMG recording and for this reason not scanned in the MRI (data not shown).

E-Cage, exercise cage; EMG, electromyogram; MRI, magnetic resonance imaging; 1.5/3T, 1.5/3 Tesla scanner; CST, corticospinal tract.

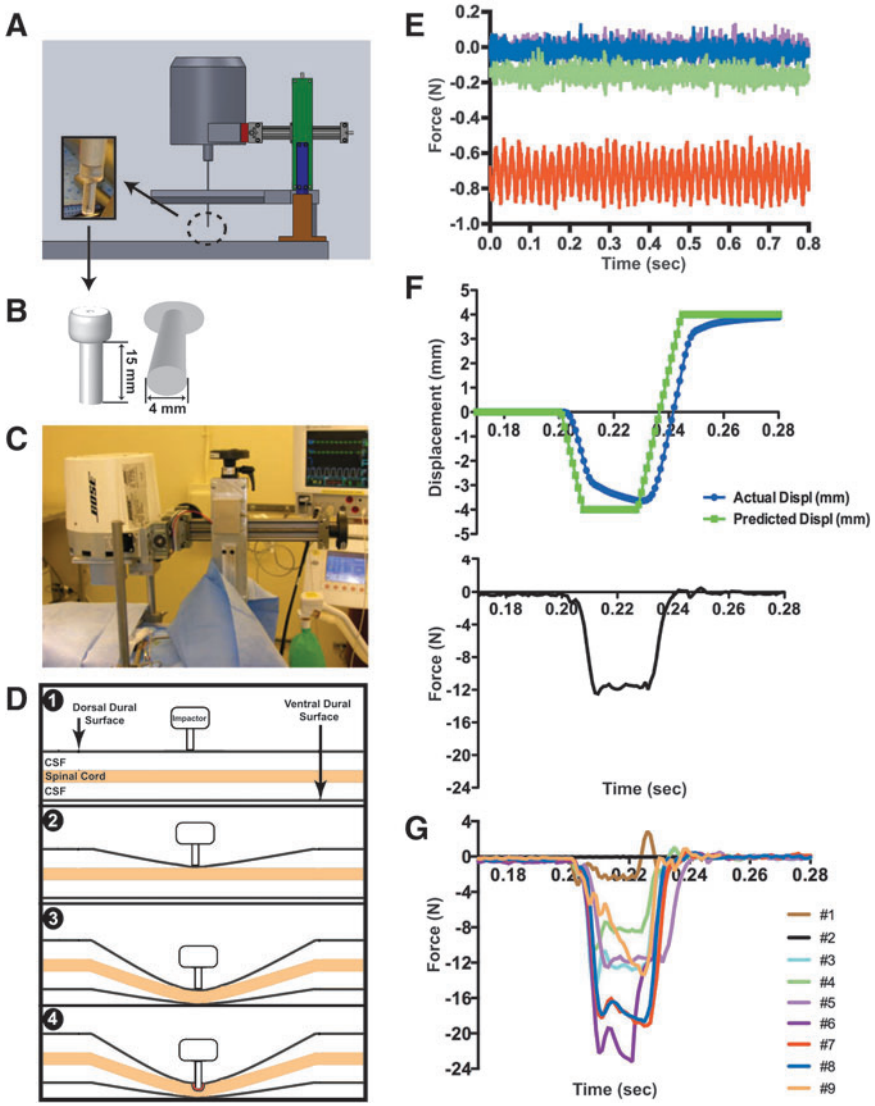

FIG. 1. The contusion device, its use and the resulting force readout for all impacts. A computer-aided design illustration of the actuator on the stereotaxic frame and spinal unit **(A)**, including the dimensions of the polycarbonate impactor tip **(B)** and *in vivo* setup during surgery **(C)**. Measures taken to stabilize the spinal cord prior to initiating impact are graphically illustrated (**D**, steps 1-4) to demonstrate initial contact of impactor tip with the dural surface followed by gradual displacement of the cerebrospinal fluid (CSF) until the cord is stabilized against the ventral aspect of the canal. A deflection in force from the compensated load readout **(E)** indicates the spatial location of the dura (D1), the spinal cord surface (D2) and the spinal cord contact with the bony canal (D3-D4). Sample readouts during surrogate testing are shown (E) to demonstrate differences in force readouts over time at each step starting with the impactor tip alone with no contact (pink trace), initial contact of impactor tip with dural surface (blue trace), displacement of the CSF and contact with the spinal cord (green trace), and displacement of CSF under the spinal cord with entrapment against the floor of the vertebral canal (red trace). Biomechanical parameters such as actual displacement (**F**, blue trace) and peak force over time (F, black trace lower graph) are available immediately after impact; these traces are from subject #5. Actual force traces for all subjects are shown in **G** (see text for details).

monitored and maintained within acceptable ranges. Analgesics, such as oxymorphone hydrochloride (0.15 mg/kg; Endo Pharmaceuticals Inc., Chadds Ford, PA), and antibiotics (cefazolin, 25 mg/kg IM; GlaxoSimthKline, Research Triangle Park, NC) were administered. A complete laminectomy at the fifth cervical vertebra (C5) was made using a Stryker drill (Impaction drill; Surgical Power, Inc. Warsaw, IN; 3.5 mm round drill bit) to expose the dura (which was not opened) and the underlying spinal cord. Laminectomy size was noted for each subject (Table 2).

Next, the Bose impactor unit was positioned over the C5 laminectomy site; the vertebral clamps were fixed to the spinous processes of C4 and C6. The impactor rod (tip 4 mm in diameter to match the size of the NHP hemi-cord at spinal level C6-7) was lowered over the right side of the cord onto the dural surface with the tangent to the circular edge of the impounder aligned along the midline (subjects #1, 2, and 9), 1 mm to the left of midline (subjects #3-7) or 0.5 mm to the left of midline (subject #8), then lowered to make direct contact with the dural surface. To confirm accurate positioning of the impounder on the spinal cord, real-time force readouts of the compensated load served as a monitoring tool to identify the dural surface, the cord surface, and the entrapment of the cord against the ventral aspect of the canal (Fig. 1D, 1E). Upon reaching a force readout indicating entrapment of the cord against the canal, the impactor displacement programmed into the Test-Bench system (set at 2, 3, or 4 mm) was initiated to produce the contusions. The force necessary to produce the set displacement

Table 2. Laminectomy Size, Impactor Positioning and Biomechanical Summary

	Subject #1	*Subject #2*	*Subject #3*	*Subject #4*	*Subject #5*	*Subject #6*	*Subject #7*	*Subject #8*	*Subject #9*
Laminectomy size AP × ML (mm)	11×7	9×7	12×8	11×8	12×9	11×9	12×7.5	12×12	11×9
Depth from dural surface (mm)	n/a	2.0	2.5	3.0	3.6	3.0	3.2	3.5	2.8
ML position (mm)	0.0	0.0	−1.0	−1.0	−1.0	−1.0	−1.0	−0.5	0.0
Set speed (m/sec)	1	1	1	1	0.5	1	1	1	1
Actual speed (m/sec)	0.27	0.27	0.55	0.55	0.42	0.48	0.51	0.51	0.58
Set displ (mm)	−2.0	−2.0	−3.0	−3.0	−4.0	−4.3	−4.3	−4.3	−4.3
Actual displ (mm)	−1.91	−1.71	−2.66	−2.78	−3.64	−3.68	−3.52	−3.46	−3.72
Time to max displ (sec)	0.02	0.02	0.02	0.02	0.02	0.02	0.02	0.02	0.02
Preload force (N)	−0.02	−0.03	−0.30	−0.30	−0.40	−0.56	−0.33	−0.28	−0.18
Force at max displ (N)	−1.64	−0.16	−12.90	−8.48	−11.07	−11.63	−19.10	−17.97	−13.40
Peak force (N)	−3.27	−4.48	−14.90	−10.54	−12.50	−23.19	−19.15	−18.73	−13.40

AP, anterior-posterior; ML, medial-lateral; N, Newton; displ, displacement; n/a, not available.

was measured and all impact biomechanical variables recorded were available immediately after the impact (Table 2). The impounder did not perforate the dura at the impact site.

In addition to system readouts, a 7 mm flexible inspection camera (Borescope, Model iT50-BT-BFBA; Brainy Trade, Passaic, NJ) was introduced into the outer margins of the incision to visually monitor the precise placement of the impounder prior to and during contusion of the spinal cord. After the contusion, the wound was closed in anatomical layers and the animal was allowed to recover under veterinary care in the hospital where they received intensive care unit (ICU) care for the first few days of recovery.

Upon release from the hospital, animals were returned to their home cages equipped with extra bedding materials to prevent pressure sores. The animals were attended every few hours during the day and encouraged to sit up, reach, and stand by offering food rewards (e.g., fruit, raisins, etc.). As soon as the animals were able to enter the transfer box, they were allowed to enter the open field exercise cage. Chairing was initiated shortly thereafter.

CST labeling. In our previous study of NHPs with cervical spinal hemisections,[11] multivariate principal components analysis (PCA) provided evidence for a role of sprouting of the intact CST in recovery. To begin to study this in the NHP contusion injury model, we labeled the CST in three animals (subjects #5, #6, and #8). Fourteen weeks after SCI, the CST was anterogradely labeled using biotinylated dextran amine (BDA) as the tracer, as previously described.[11,19] Briefly, under deep anesthesia as described above for the spinal surgery, a craniotomy was performed and the dura was incised and retracted to expose the motor cortex. A glass micropipette fixed to a picospritzer was used to inject 0.3 μL of BDA (10%) at 59 sites (127 total injections) throughout the left primary motor cortex serving the hand, trunk, and foot. The wound was closed in anatomical layers and the animals were allowed to recover under veterinary care in the hospital where they received ICU care for the first few days of recovery. Six weeks after labeling, animals were intracardially perfused with fixative under deep anesthesia and processed for histological evaluation.

Open field behavioral testing

Exercise cage. All animals ($N=9$) were scored in an open field task developed to assess general motor function and overground locomotion, climbing, and object manipulation.[12] Animals entered a large open wire-mesh cage (7 feet [height] ×10 ft [width] ×6 ft [depth]) through a chute where they had the option of ascending a series of four elevated perches to reach a food reward placed inside a Kong® (a hollow rubber toy filled with food such as peanuts, raisins, small pieces of dried fruits, etc.; The Kong Company, Golden, Co), on the top perch. Locomotor activity was evaluated while the animals traversed the perches, as well as on the floor of the open cage. Climbing was assessed during food retrieval from a series of five cups hanging at different heights (1.5, 2.7, 3.5, 4.3, and 4.7 ft) on the front of the cage. Object manipulation was assessed during manipulation of the Kong® (hollow toy) and during

Table 3. Open-Field Scoring Scheme

Category	*Subscore*	*Max score*	*Score composition*
Locomotion		34	Overground locomotion and walking
	General	(10)	Forward movement (dragging-walking), number of limbs used, number of perches reached, presence/absence of tremor, ability to touch head/face with forelimb
	Movements and weight support	(10)	Ability to move upper (shoulder, elbow, wrist, fingers) and lower joints (hip, knee, ankle, toes), weight support during stance or sitting
	Walking	(14)	Foot faults, placement surface, stepping and gait asymmetry
Climbing		16	Forelimb (wrist, fingers) or hindlimb (heel, toes) joints used during climbing and retrieval, finger/toe strength, number of cups reached
Object manipulation		22	Predominant joint position of forelimb and hindlimb during object manipulation, forelimb support of object on and off ground, joint and independent finger movements, digit 1 opposition and frequency, pincer grasp
Total		72	

the consumption of a large food item (e.g., apple or orange). Body and limb posture, wrist, hand, and individual finger movements were assessed during manipulation of the objects both on and off the ground. Scoring of functional recovery was similar to that described by Nout and colleagues,[12] where behavioral features were assigned 0, 1, or 2 points, with the highest point assignment representing normal function (see Table 3 for a summary description of the scoring system, supplementary Fig. S1 for the data collection sheet, and supplementary Fig. S2 for the specific point assignment schema; see online supplementary material at www.liebertpub.com). Animals were placed in the exercise cage 4-5 times/week; two testing sessions per week were performed as described above and were recorded; at least one session/week was scored live.

Chair tasks

A subset of animals (subjects #5, #6, #7, and #8) was tested in a primate chair for isolated use of the forelimb ipsilateral to the lesion. Animals were pre-trained to enter and exit the restraint chair using a pole-and-collar system. Upon successful completion of this training, animals were trained to perform the separate tasks described below. For each task, the proportion of trials with successful completions (i.e., successful transfer of food rewards to the mouth) is reported. Chairing occurred three times/week, with the first two sessions being training/re-training sessions and the last session being the testing session.

Assessment of tone. At the beginning of each post-operative chairing session, the affected forelimb was gently massaged, joints were moved through the full range-of-motion, and muscle tone was rated using the Modified Ashworth Scale,[20] where 0 = no increase in muscle tone, 1 = slight increase in muscle tone (manifested by a catch followed by minimal resistance through the remainder [less than half] of the range of motion), 2 = slight increase in muscle tone (manifested by a catch followed by resistance through greater than half of the range of motion), 3 = more marked increase in tone throughout most of the range of motion but the affected part is easily moved, and 4 = the affected part rigid in flexion or extension. An aggregate score was determined by assessing the elbow, wrist, and finger joints.

Platform retrieval task. Animals were trained to retrieve a small or medium-sized food reward (i.e., raisin, peanut, or grape, apple piece, etc.) from a flat platform positioned so that only the impaired limb could be used for item retrieval. Five trials per reinforcer size per session were conducted.

Stick retrieval task. Animals were trained to retrieve a food item (e.g., a grape) from a vertical post/stick positioned in the center of the flat platform. Five trials per session were conducted followed by a second set of five trials with an inverted funnel placed over the stick/post forcing use of a pincer motion for retrieval.

Handle pull task. In this task, animals were trained to pull a U-shaped handlebar attached to a spring with force tension of 20 Newton (N; easy), 60 N (medium), or 98 N (hard). The handle was oriented in a horizontal and then vertical position and the animal's performance was assessed in a total of three trials in each position per session with a constant spring force predetermined by the level of impairment and ability of the animal to perform each task.

Brinkman board. In this task, animals retrieved small-sized food items from a Brinkman board containing 7 slots (3.5 cm long ×1 cm wide ×0.5 cm deep), four vertical, one horizontal, and two angled at 45°. The board was loaded twice for a total of 14 trials.

Assessment of sensory function using an electronic von Frey apparatus. Subjects were trained with positive reward to sit quietly in the restraining chair adapted with a custom-made winged bib to occlude views to the side and below the subject's neck where a tester was positioned. Five 1 mm stimulation sites on each side of the animal were marked with indelible ink (see schematic in Fig. 7A): shoulder (C4 dermatome), lateral hand (C8 dermatome), mid-thorax (T10 dermatome), lateral knee (L3 dermatome), and lateral foot (S1 dermatome). An electronic von Frey apparatus (Model 2390; IITC Life Science, CA) with a 10-g bending force filament attached was used to stimulate each site (three stimulations /site) in a random order. Alternate false alarm trials were interposed, and responses were recorded for all trials. The inter-trial interval was approximately 15 sec. For video recording purpose, stimulus onset was light-cued using a light-emitting diode positioned behind the animal, out of its field of view. The stimulus was applied with a slow onset and was held for approximately 1.5 sec before being withdrawn. Responses were recorded by an observer positioned in front of the animal with a clear view of the animal's face and body. Maximal force for each stimulation was recorded, as were the following specific responses: vocalization, wince, orientation, activity arrest, flinch/skin contraction, withdrawal, and no response. Preferred food items were given at variable times during the session by another experimenter to reinforce sitting quietly. This bi-weekly session usually lasted between 10-15 min. For analysis, data were binned into three time-points (4 and 5, 9 and 10, and 15 and 16 weeks post-lesion) representing the early, mid, and late recovery periods, respectively. Response data also were binned into four categories: 0 = no response; 1 = segmental or spinal responses (withdrawal, skin contraction or flinch); 2 = suprasegmental or supraspinal responses (orientation, activity arrest); and 3 = facial supraspinal responses (wince and vocalization).

Magnetic resonance imaging

Magnetic resonance imaging (MRI) scans were obtained post-operatively for four subjects (Table 1) at 14–17 weeks after SCI, and pre-operatively, as well, for cases #8 and #9. Animals were sedated with ketamine (Ketaset 10 mg/kg [to effect range, 5–30 mg/kg], intramuscularly (IM); Mylan Institutional LLC) and atropine (0.05 mg/kg IM; Baxter HealthCare Corp.), intubated, and maintained using isoflurane (1.5–2.0%; Piramal Critical Care Inc.). Animals were placed in an MRI-compatible stereotaxic device (Model 1430 M; David Kopf Instruments). Pre-operative MRIs were obtained to estimate the cord and CSF space size for matching to the mechanical readouts of the contusion device signaling dural touch, cord touch, and cord stabilization; this is now the standard procedure (Fig. 2).

1.5 Tesla System. A 1.5-T GE scanner (GE Medical Systems, Waukesha, WI) was used to acquire magnetic resonance images on three subjects, and were collected using two 3-inch round coils placed dorsally and ventrally over C6 (Model 2127315, GE Medical Systems, Milwaukee, WI). In addition, NHPs were imaged with a Knee Array (Model 5114356-5; InVivo Corporation, Gainesville, FL) positioned in a supine/prone position. For the 3-inch coils, the field of view (FOV) was set at 14 mm, 0.0 mm spacing, and a slice thickness of 1 mm. For the knee array, the FOV was 16 mm, 0.0 mm spacing, and a slice thickness of 2 mm. Acquisition of magnetic resonance images started with sagittal and axial T2-weighted fast relaxation fast spin echo at 1 mm slice thickness followed by T1-weighted sequences acquired on both planes and thicknesses.

3 Tesla system. To improve image quality and optimize new MRI protocols, one subject was imaged in a 3T Siemens MAGNETOM Skyra scanner using a custom-built four-channel Clamshell MRI coil (Model P-H04LE-030-01295 V01; Rapid MR International, Columbus, OH). Magnetic resonance images acquired on this system included high-resolution 3D T1- and T2-weighted isotropic scans oriented in the sagittal plane with a slice thickness of 270 μm.

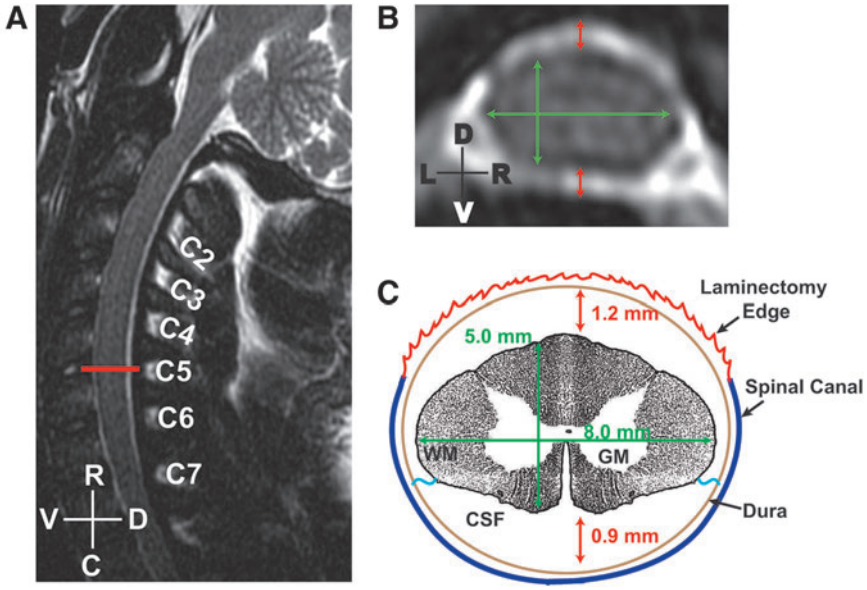

FIG. 2. Pre-operative magnetic resonance images used to generate measurements of the spinal cord parenchyma and cerebrospinal fluid (CSF) space. Sagittal **(A)** and axial **(B)** T2-weighted images acquired on a 1.5T scanner indicate the location of the fifth cervical vertebral level (A, red line) and were used to estimate size of the spinal cord (B, green lines) and amount CSF space (A, red lines) at that level. Based on these approximations, a schematic representation for the region of interest was generated **(C)**. In this example, measurements of spinal cord (5×8 mm) and CSF spaces 1.2 mm above and 0.9 mm below the spinal cord) are shown, as well as a representation of the projected laminectomy, the vertebral canal, and the denticulate ligaments (blue wavy lines). R-C, rostral-caudal axis; D-V, dorsal-ventral axis; L-R, left-right side; W/GM, white/gray matter.

Three-dimensional volume reconstruction. Reconstruction of lesion volumes was conducted using OsiriX® software (v5.5.2). Briefly, the regions of interest (ROIs), defined as the regions of high intensity signal as observed on T2-weighted magnetic resonance images, were manually traced on each of the MRI slices in OsiriX and were then reconstructed using an automated ROI volume tool.[21]

Necropsy

Survival time varied with each subject and was determined by behavioral plateau (#1-4) and then by plateau followed by cortical labeling plus 6 weeks for BDA transport. Animals were sedated with ketamine (5-30 mg/kg IM; Mylan Institutional LLC) followed by induction of a deep plane of anesthesia using pentobarbital (approximately to effect 60 mg/kg intravenously; Vortech Pharmaceuticals, Dearborn, MI). Animals were then transcardially perfused with 1% paraformaldehyde (PFA) in phosphate-buffered saline (PBS) for 10 min followed by 4% PFA/PBS for 45 min. Tissues were post-fixed in 4% PFA/PBS overnight and transferred into 10% and then 20% glycerol with 0.2% dimethyl sulfoxide/1% phosphate buffer.

Tissue processing

Spinal cords were collected and cut into blocks corresponding to spinal segments identified by locating the entry zone for each dorsal root and cutting just rostral to the entry zone. The arachnoid membrane was removed prior to sectioning. Serial sections were cut at 40-μm on a Leica sliding freezing microtome (HM-450; Fisher Scientific, Clifton, NJ) and were placed in cryoprotectant solution until processed for histological analysis. Brains also were collected and in cases with cortical labeling, cut frontally into 5 mm blocks and frozen for later sectioning.

Histology

Eriochrome cyanine staining for myelin. Pre-dried slide-mounted sections were placed in 100% alcohol:chloroform (1:1) for 1 h, washed in 100% alcohol (2×1 min), air dried at room temperature (RT), and stained in eriochrome cyanine (EC) solution for 20-30 min, then washed in running tap-water. After washing, slides were differentiated in 5% iron alum solution at RT (15 min), washed in running tap-water, differentiated in borax-ferricyanide at RT (10 min), washed again in running tap-water and counterstained in 0.5% neutral red (NR) for 1-2 min at RT before a final wash in water. Sections were dehydrated in graded alcohols (70%, 95%, and 100%; 2×2 min each), submerged in xylene (2×5 min) and cover-slipped with Shandon-Mount (#44581; Sigma, Waltham, MA).

BDA staining for CST tracing. Sections were washed in Tris buffer solution (TBS, pH 7.4; 3×10 min), incubated in 0.6% H_2O_2/100% methanol at RT (30 min), washed again in TBS (3×5 min) and incubated overnight at 4°C in TBS +0.25% Triton-X (BP151-100; Fisher Scientific) containing Vector ABC elite solution (9 μL/mL reagent A +9 μL/mL reagent B, PK6100; Vector Laboratories, Burlingame, CA). The next day, after washing in TBS (3×10 min), sections were developed with DAB (2.5 min; SK-4100, Vector Laboratories), washed in TBS (3×5 min), mounted on slides, dehydrated and cover-slipped with Shandon-Mount.

Histological analysis of lesion parameters and tissue sparing

Calculation of lesion length, volume, and tissue sparing at the lesion epicenter was performed on spinal cord sections co-stained for myelin with EC and for cell bodies with NR. The lesion epicenter, identified by two independent observers, was indicated as the section with the greatest damage (estimated by the overall loss of gray and white matter). Using the epicenter as the starting point, lesion measurements were taken from the section at the epicenter and at ±1.6 and ±3.2 mm rostral and caudal. Brightfield images were captured (BZ-9000; Keyence, Woodcliff Lake, NJ) at a resolution of 2000×1000 pixels and merged using image analysis software (BZ-II; Keyence). Images were divided into sectors in Adobe Photoshop

(CS4, v11.0.2, Adobe Systems, Inc., San Jose, CA), using a superimposed 16-split circle (the ventral artery and dorsal median sulcus served as the reference landmarks), and color-coded to represent the ROI (lesion, red; gray matter, blue; white matter, green). Pixel counts were analyzed in MetaMorph(MetaMorph Inc., Nashville, TN) and then converted to mm^2 in Excel(Microsoft Office 2010, Microsoft Corp., Santa Rosa, CA; e.g., mm^2 = number of pixel/1872 pixels per 2 mm). Since the lesion produced distortion and shrinkage of the cross-sectional area of the spinal cord, a section 4.8 mm rostral from the lesion epicenter was used as a comparison to derive proportional epicenter calculations. Lesion volume between measured sections was calculated using the formula for determining the volume of a frustrum of a cone as previously described.[22] The total amount of spared tissue is presented as a percentage of the entire cross-sectional area of the spinal cord (spared tissue/cord area ×100).

Statistical analysis

As part of the validation of the contusion model, exploratory data-driven analytics were performed to test for associations between biomechanical parameters, lesion pathology and tissue sparing, and functional outcomes. Bivariate correlations were assessed for all pairwise comparisons. In addition multivariate correlation was assessed using PCA or its non-parametric equivalent (categorical PCA), as needed. All analyses were performed in SPSS v.21 (SPSS Inc., Chicago, IL) using base, regression, advanced models, categories and missing values add-ons.

Ashworth scale data were analyzed using generalized estimating equations, with an ordinal link function to measure changes in the ordinal categories of the Ashworth response (0-5) over time (weeks post-lesion, 2-13) using repeated measures. Linear mixed model was used to calculate the estimated marginal means (EMM) for display purposes only. Statistical significance was set at $\alpha = 0.05$.

For analysis of sensory function using the von Frey apparatus, data were binned across three time-points (4 and 5 weeks, 9 and 10 weeks, and 15 and 16 weeks) post-injury. Maximum force data were analyzed using a four-way nested repeated measures general linear model (analysis of variance [ANOVA]). Response category data were first grouped into four categories, with each category having an assigned number: 0 = no response; 1 = spinal response (flinch/skin contraction, withdrawal); 2 = supraspinal response (activity arrest, orientation towards stimulus); and 3 = facial supraspinal response (wince or grimace, vocalization). These data were then analyzed using generalized estimating equations with an ordinal link function to measure changes in the ordinal categories (0-3) over time using repeated measures. This is the nonparametric equivalent of a 4-way nested repeated measures general linear model (ANOVA). Significant main effects and interactions on the generalized estimating equations were followed up using *post hoc* procedures of cross-tabulated chi-square to assess specific response categories. A generalized linear model was used to calculate the estimated marginal means for display purposes only. The maximal force applied was used as a covariate in both the generalized estimating equations and the generalized linear model procedures. Statistical significance was set at $\alpha = 0.05$.

Results

Deriving optimal impact procedures

Initial tests with the surrogate silicone model of the spinal cord suggested that a 2 mm displacement would be optimal for a mild injury. However, the first two subjects we impacted with the depth set to 2 mm showed no signs of damage. In addition, the force readouts suggested that the cord provided little resistance to the impact, perhaps moving only within the CSF space or perhaps slipping from under the impounder during impact (Fig. 1G, black and brown lines). Either event could be due to the large CSF compartment around the spinal cord in primates, a fundamental difference from the rodent model, which has a low proportion of the canal occupied by CSF space. At this point, the surrogate cord model was expanded to include a CSF component and the impact procedures were modified as shown in Figure 1D. This procedure, intended to establish a consistent starting and ending point, was used for all subsequent animals.

Force readouts from the compensated load cell were used as ''position guides'' indicative of displacement of CSF and spinal cord entrapment. Increments in force, associated with advancement of the impactor, were first tested on the surrogate cord. These force increments indicated the spatial location of the impactor, reflecting (in order): 1) dural contact, 2) cord surface contact, and 3) cord contact with the base of the canal.[17] As illustrated in Figure 1D and 1E, the initial contact of the impactor with the dural surface generated a slight negative shift in the force readout from baseline (Fig. 1D, step 1; Fig. 1E, pink trace) and this was confirmed visually. Further advancement of the impactor (by 1.0 to 1.5 mm) created a second distinct shift in force as the impounder contacted the dorsal aspect of the cord (Fig. 1D, step 2; Fig. 1E, blue trace) and displaced CSF as contact with the spinal cord was made (Fig. 1D, step 3; Fig. 1E, green trace). Additional advancement (by 1.0 to 1.5 mm) caused contact of the spinal cord with the floor of the vertebral canal, and was signaled by an increased shift in force (Fig. 1D, step 3-4; Fig. 1E, red line).

The advancement at each of the aforementioned levels reduced CSF space first dorsally and then ventral to the spinal cord, providing a consistent starting point for impacting the cord (Fig. 1D, step 4). No adverse changes in vital signs were detected during this slow entrapment of the cord prior to impact. The final force reading for this procedure is reported as the ''pre-load force'' in the data described below. In the later animals with pre-operative MRIs (subjects #6, #8, and #9), these specific increments were matched to the measurements calculated from the baseline magnetic resonance images as shown in Figure 2. Thus, each animal with pre-operative MRIs had the procedure individualized to their own measurements.

Upon satisfactorily pressing the cord to the bottom of the canal (Fig. 1D, step 3), a rapid cord impact was initiated (Fig. 1D, step 4). Biomechanical data acquired immediately after each impact was collected and analyzed using the Wintest® (v7.0; Bose Corporation, Eden Praire, MN) control software. An example of impact data from subject #5 is shown in Figure 1F; contusion depth was set at 4 mm from the start position on the cord surface at a set speed of 0.5 m/sec using the indicated waveform, and the resulting measured displacement of the impounder is shown by the blue line (Fig. 1F). The speeds used in this contusion model were at the maximum capacity of the Bose TestBench System; therefore, although the displacement was set to occur over 20 msec, there was some variation in the test results. In this particular case, maximal displacement (-3.64 mm) occurred 23 msec after initiation of the pulse, and resulted in a peak force of 12.5 N (lower graph, black line). The force curves for all impacts ($N = 9$) are shown in Figure 1G. The biomechanical impact parameters for all subjects are presented in Table 2.

The Bose TestBench software and the Bose device allow for setting either displacement or force as the feedback control signal. We chose to control/pre-set displacement. The resulting forces for the different subjects are shown in Table 2. The relationship between displacement, the resulting force, and the outcomes is described and evaluated below. Over the course of the study, we increased displacement settings from 2.0, to 3.0, and then to 4.0 mm with intended speed set at 1 m/sec (except for subject #5,

where the speed was set at 0.5 m/sec; Table 2). All of these impacts, with the exception of the first two subjects, produced a profound immediate post-operative paralysis of the right side (same side as the lesion), which improved to varying degrees over time. Subjects were usually able to return to their home cages within a few days after injury, and were able to enter the transport box and move into the open field exercise cage within two weeks (except for subject #7). A more detailed account of the behavioral tasks and recovery is given below.

MRI

MRI was performed in the later subjects and provided valuable pre-operative information on cord size, canal size, and CSF space (Fig. 2), and post-injury assessment of contusion lesion size that was later matched to the corresponding histology (Fig. 3). Three subjects were imaged on a 1.5 T (subjects #5, 6, and 8) and one on a 3T scanner (subject #9; Fig. 3) peri-operatively. The pre-operative images served as planning tools providing estimates of the dimensions of the spinal cord and CSF space at the fifth cervical vertebral level (Fig. 2) as mentioned above. High-resolution T2-weighted sagittal images (slice thickness 1 mm or 270-μm, respectively) were acquired to identify the ROI (Fig. 2A), and the corresponding axial view (Fig. 2B) was utilized to measure the CSF space and the cord dimensions (Fig. 2C). The representative sample shown here indicates that the spinal cord measured 5.0 mm dorsoventrally and 8.0 mm mediolaterally. In addition, the CSF space on the dorsal surface of the cord was estimated at 1.2 mm and 0.9 mm on the ventral side. These values were used to estimate the dorsoventral excursion of the impactor from the dural surface necessary to trap the cord before impacting (Fig. 1D) and correlated well with the preload force protocol applied during the surrogate impact.

Post-operatively, the contusion injuries appeared as hyperintense areas on T2-weighted MRI sequences (Fig. 3, red arrows). Sagittal and horizontal images demonstrate the rostro-caudal spread of the hyperintense T2-signal and axial images show the medio-lateral spread. High intensity T2-weighted signal is generally considered to represent regions of high fluid content, and thus may correspond to the lesion cavities seen later in histological sections (Fig. 3 and Fig. 4). However, comparisons between the lesion volume in the MRI and the histological sections indicated that the rostro-caudal extent of the lesion was underestimated by the T2 hyperintense signal. The axial images at the lesion epicenters were a closer match (Table 4). This discrepancy is not surprising since various amounts of cavitation and cellularity in the lesion were seen in the histology. Volumes estimated from the T2 hyperintense signal did, however, yield estimates of lesion volumes that have proved useful in planning for cellular transplants (as part of a separate study).

Lesions and tissue sparing

Rapid impact with the Bose actuator under displacement control produced large, mostly unilateral contusion lesions that looked

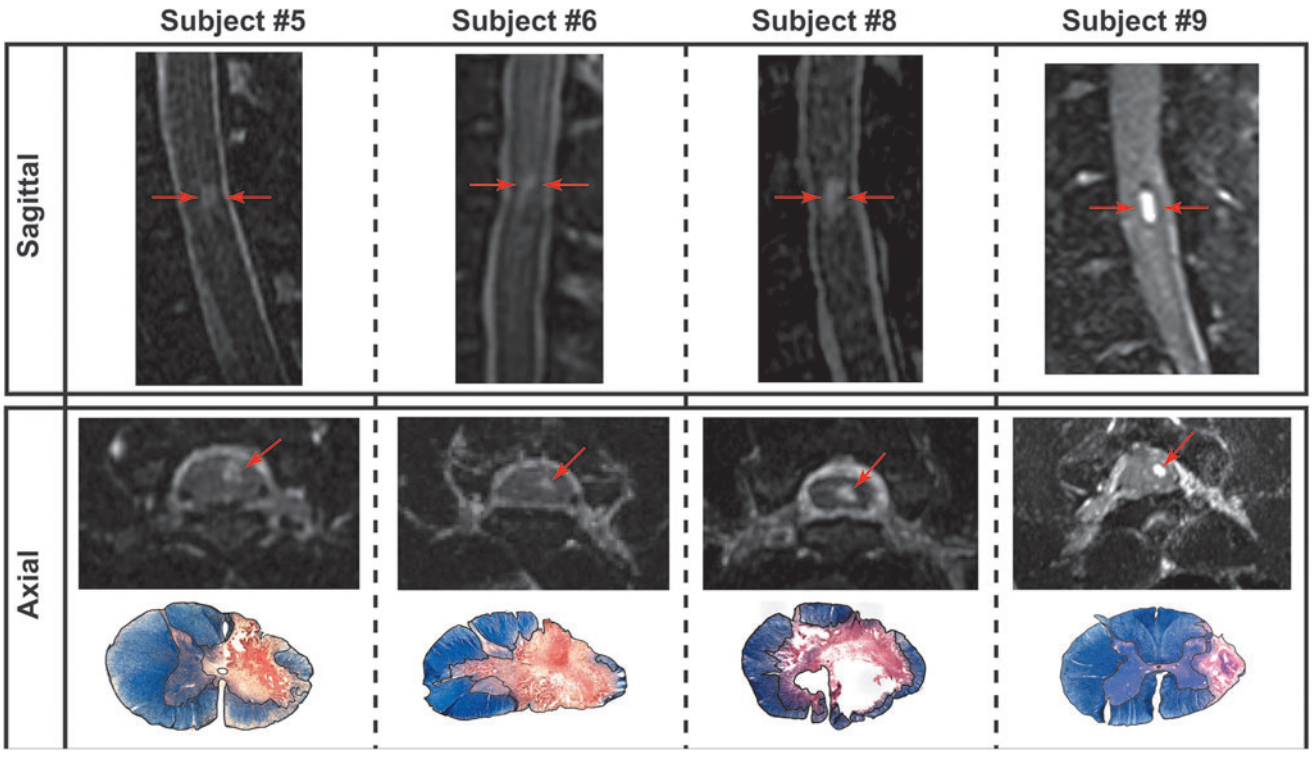

FIG. 3. Post-lesion T2-weighted magnetic resonance images of the spinal cord used to identify the lesion area. Animals were imaged on a 1.5T scanner (subjects #5, 6, and 8) or on a 3T scanner (subject #9). Single magnetic resonance imaging (MRI) slices in the sagittal and axial plane demonstrate the region of hyperintensive T2-signal indicative of the lesion (red arrows). For comparison, the lesion epicenters identified in the histological sections (stained with eriochrome cyanine and neutral red) also are shown. The MRIs were performed at 14 or 17 weeks after injury, and sacrifice was at 19, 20, or 21 weeks after injury (Table 4). The larger lesion size in the histological sections is noteworthy and may reflect the high density of cellular elements in the lesion site as reflected by the neutral red staining, whereas, hyperintensive T2-signal from the magnetic resonance images was limited to the fluid filled cavities, and these were not so clearly evident in the histological sections.

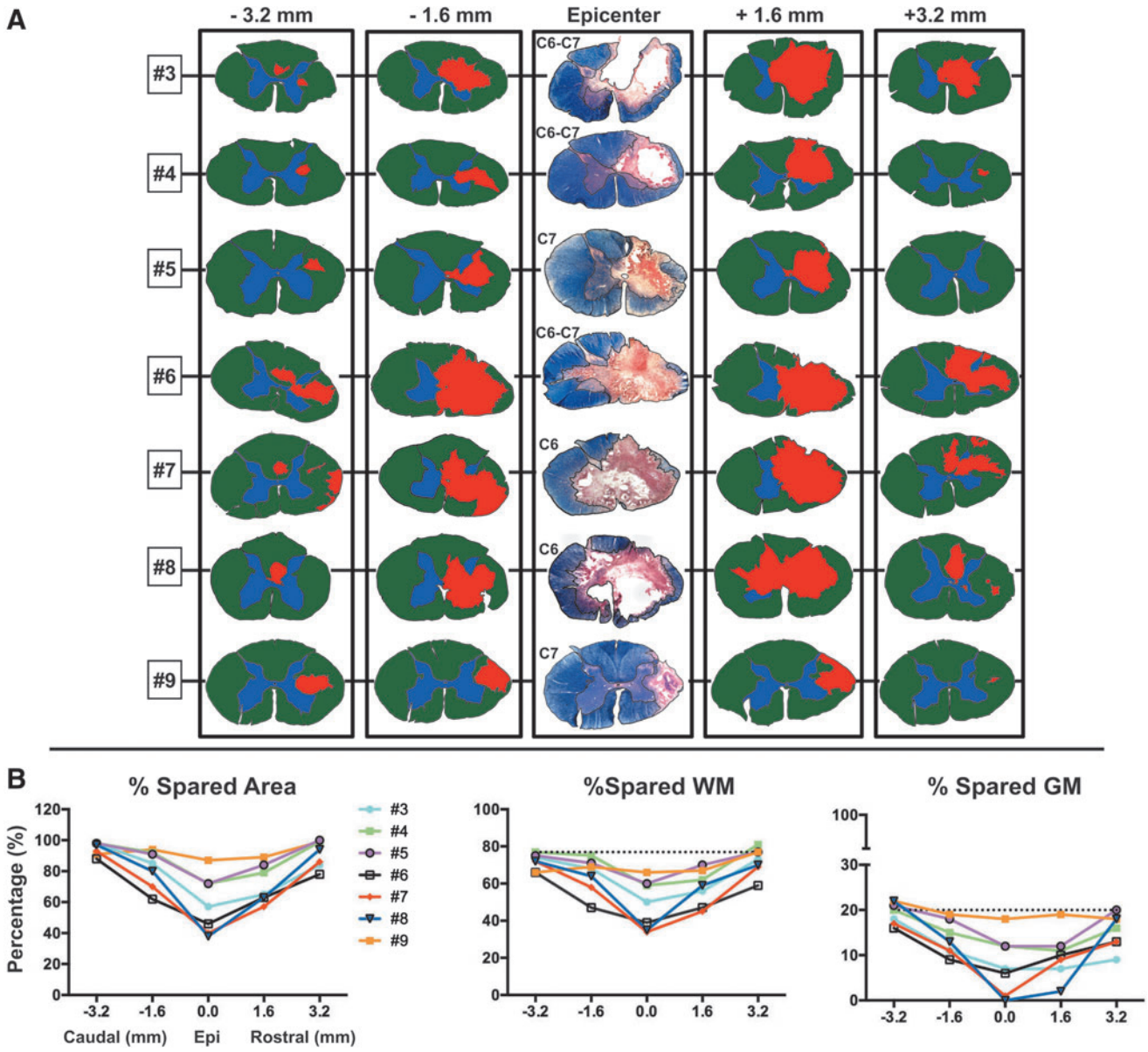

FIG. 4. Histological section analysis of the rostral-caudal spread of the lesions shows that the more severe lesions extend for considerable distances in the spinal cord and affect both white matter (WM) and gray matter (GM) areas. **(A)** Histological sections processed for eriochrome cyanine and neutral red were used to reconstruct the spread of the lesion, and are shown for all injured subjects at the lesion epicenter and at 1.6 and 3.2 mm rostral and caudal. For measurement purposes, sections at the aforementioned intervals were drawn and color-coded in Adobe Photoshop (gray matter = blue; white matter = green; lesion area = red). The graphs in **(B)** show quantification of the total lesion area at all intervals. Total gray and white matter sparing, as well as total spared area, are represented as a proportion of the entire cross-sectional area of the spinal cord, and the dotted lines represent the percent of gray and white matter in an uninjured cord section.

similar to those produced in our model of unilateral cervical contusion injuries in rats.[7,14,23] In general, subjects receiving a 3 mm pre-set displacement injury had smaller lesions (Table 4) and the best recovery. Subjects receiving 4 mm pre-set injuries had larger lesions, with the exception of subject #5, which had a pre-set speed of 0.5 m/sec (and an actual speed of 0.42), and subject #9, which had a spinal deformity (scoliosis) that we suspect resulted in an angled impact. Note also that subject #9's peak force was much less than that of subjects #6, #7, and #8, and the also impact was more lateralized (impactor tangent was positioned at the midline rather than 1 mm over). Thus, the 4 mm displacement setting produced a large lesion on the ipsilateral side with some extension across the midline. Lesion volumes and sparing data are given in Table 4 and Figure 4. Lesion length along the rostro-caudal axis ranged between 0.56 cm and 1.2 cm, and between 0.03 cm^3 to 0.09 cm^3 in volume (Fig. 4A).

Relationship between biomechanics and lesion size

There is a complex relationship between displacement, peak force, and the other measured biomechanical parameters that depends in part on tissue stiffness, cord and spinal column morphology, and perhaps unknown factors, as well.[17] To examine the

Table 4. Measures of the Lesion

	Subject #3	*Subject #4*	*Subject #5*	*Subject #6*	*Subject #7*	*Subject #8*	*Subject #9*
Histological measures							
Lesion length (cm)	1.12	0.56	0.64	1.16	1.28	0.96	1.16
Lesion volume (cm^3)	0.07	0.03	0.03	0.09	0.08	0.08	0.04
Lesion area at epi (mm^2)	13.63	9.69	10.73	17.17	18.30	25.08	4.15
% Spared GM at epi	33	58	61	28	5	0	88
% Spared WM epi	47	58	72	50	33	49	74
% Spared area at epi	44	63	69	40	29	37	74
MRI measures							
Time of MRI after SCI (weeks)	n/a	n/a	17	14	n/a	17	14
Time of necropsy after MRI (weeks)	n/a	n/a	20	21	n/a	20	19
Lesion length (cm)	n/a	n/a	0.31	0.33	n/a	0.34	0.30
Lesion volume (cm^3)	n/a	n/a	0.014	0.013	n/a	0.021	0.005
Lesion area at epi (mm^2)	n/a	n/a	5.36	5.85	n/a	5.68	2.03

Epi, epicenter; GM, gray matter; WM, white matter; MRI, magnetic resonance imaging; SCI, spinal cord injury.

relationships between mechanics, lesion size, and behavioral outcome at the end of the experiment, we performed both bivariate correlations and a multivariate analysis. Lesion size, including volume, length, and area at the epicenter, are best predicted by peak force (e.g., $r = -0.932$ for lesion volume) and force at maximum displacement ($r = -0.621$ for lesion volume). This is consistent with many earlier studies of the biomechanics of contusion injury.[22,24] Figure 5 shows the correlation matrix as a heat map (higher density colors reflect higher correlations), with the specific scatter plots showing the data distribution for each relationship depicted in the cells on the lower and left sides. The center diagonal shows the data distribution for each variable; most were approximately normally distributed. The specific numeric correlations for all variables are mirrored on the upper and right sides.

Behavioral outcomes

The open field exercise cage allowed subjects to walk, climb, and manipulate food and other objects in a spontaneous way, effectively an ''activities of daily living'' (ADL) measure for monkeys (Table 3).[12,13] The overall pattern of behavioral outcome, expressed as a percentage of total possible points given for normal function, revealed a clear initial deficit when first tested after SCI (Fig. 6A) for all subjects (except for the nearly uninjured subjects #1 and #2, as previously noted). Open field scores early after injury were well predicted by the impact parameters, especially peak force (Fig. 10B). However, over the long-term course of recovery, subjects separated into two groups: those that had an initial motor deficit but spontaneously recovered well overall (subjects #3, #4, #5, #8, and #9) and those with the worst initial deficits that persisted over time (subjects #6 and #7). The different subcomponents of the open field scorings for each subject are shown in Figure 6B-D. Subjects with large lesions (subjects #6 and #7) showed the poorest recovery on all of the open field tasks. Although both cases showed some recovery of over-ground locomotion and climbing, they showed almost no recovery of object manipulation. Those subjects also showed the poorest performance in the chair tasks, as described below (Fig. 6E-H).

To provide more detail on forelimb and digit function, a subset of animals (subjects #5, #6, #7, and #8) was tested while seated in a standard primate-restraining chair. All four subjects demonstrated an initial inability to successfully retrieve and transfer food items to their mouth. The two subjects that recovered function by 4-5 weeks post-lesion, as assessed in the open field exercise cage (subjects #5 and #8) also were able to successfully perform the platform task by 5 weeks after lesion, the stick task by 6 weeks, and the handle pull task by 9 weeks (Fig. 6E-G). Consistent with the results in the exercise cage, subjects #6 and #7 performed poorly in the chair tasks, particularly in the handle pull, followed by stick and platform tasks. While subjects #5 and #8 recovered an equal ability to complete these three tasks, their Brinkman board performance highlighted a notable and continuing deficit in the ability to use a pincer grasp. Subject #8 gradually improved in this task and subject #5 was more successful, especially later in the recovery period (Fig. 6H). Nevertheless, both of these animals showed a deficit in this task at post-operative times when they were totally successful at the other tasks. This suggests that the Brinkman board provided a more sensitive measure of digit recovery than the other chair tests.

Sensory testing with von Frey hair (VFH) stimulation

The same four subjects that were tested in the chair for forelimb motor function also were tested for sensory function. The von Frey testing procedure was adapted from a previous protocol used in the rat,[25] but the up-down method using a series of von Frey filaments with different stiffness was not used for practical reasons. Instead, we used an electronic von Frey device with a constant stiffness filament (10 g) and a force transducer that provided a readout of maximal force. Pre-operatively, the overall probability of responding to the tactile stimulations was 0.52 ($n = 3$; one subject was not tested pre-operatively). Post-SCI, the probability was 0.48 ($n = 4$). The pre-lesion mean maximum force to elicit a response was 15.35 g ± 1.2 standard error of the mean (SEM) at the shoulder (range, 12.95 to 17.76), 7.08 g ± 1.2 at the hand (range 4.68–9.48), 26.66 g ± 1.2 at the thoracic site (range, 14.26–19.06), 19.78 g ± 1.2 at the knee (range, 17.38–22.18) and 15.36 g ± 1.2 at the foot (range, 12.93–17.73). The response category distributions pre- and post-operatively are shown in Figure 7B. No wince or vocalization responses were observed during any of the von Frey filament stimulations in any animal; therefore, the suprasegmental response category only contains orientation or activity arrest. The statistical analysis of the post-operative maximum force data (Fig. 7C) showed a significant main effect of time ($F[2,117] = 7.878$; $p < 0.001$), location ($F[4,62] = 61.797$; $p < 0.001$), and a time by

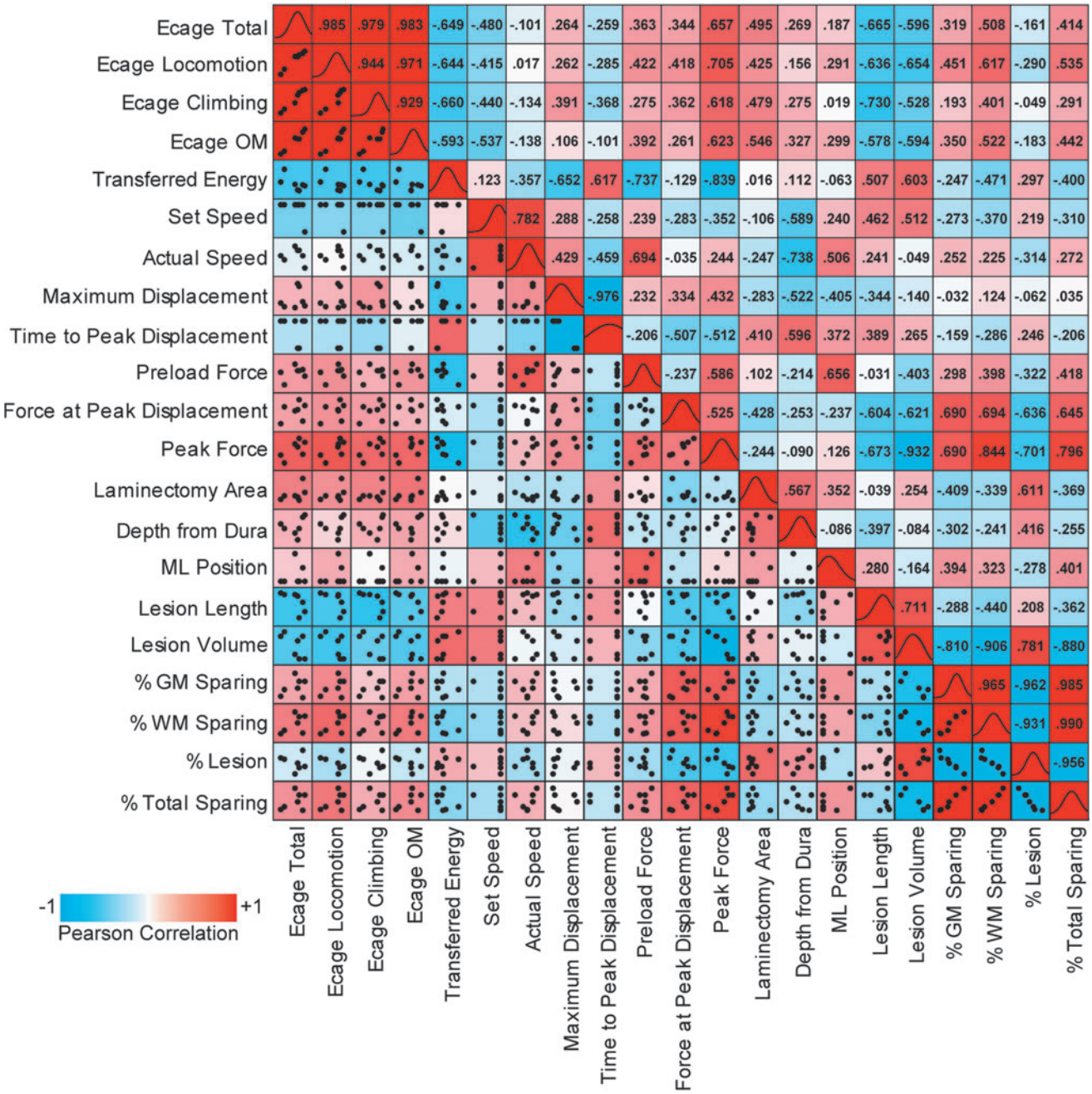

FIG. 5. Heat map of the correlational matrix showing the linear relationship of all biomechanical measures with all histological and behavioral outcome measures. Peak force and force at peak displacement correlate well with nearly all of the biomechanical, histological measures, and behavioral outcomes as indicated by the brightness of the blue and red boxes across all comparisons. Positive correlations are indicated as red and negative as blue, whereas the purity of the color is determined by the strength of the correlation (rho). Boxes on the left and lower portion of the matrix show the scatter plots of all the data. The diagonal boxes where each variable intersects itself, contains a graphical representation of the data distribution; most are normally distributed but some are clearly skewed. Boxes on the upper and right side show the specific correlation.

location interaction ($F[8,50] = 3.567$; $p < 0.002$) indicating that the force to elicit a response was slightly less over time, and the hand was the most sensitive site (Fig. 7C, orange line).

The statistical analysis of the response category data post-injury using generalized estimating equations revealed that both time and trial within sessions affected the von Frey response category (main effects: Wald chi-square = 11.146, $p = 0.004$ and Wald chi-square = 47.450, $p < 0.0001$, respectively). The probability of making a response changed over trials within a session, perhaps indicative of habituation (data not shown). The effect of trial also varied by time-point of assessment (trial × time effect: Wald chi-square = 1.227 × 10E14, $p < 0.0001$). Further, the five body locations assessed behaved differently over time (time × location effect: Wald chi-square = 2.197 × 10E13, $p < 0.0001$; Fig. 7D) and between the contra-lesional and ipsi-lesional side (time × location × side effect: Wald chi-square = 3.138 × 10E11, $p < 0.0001$). The effect of

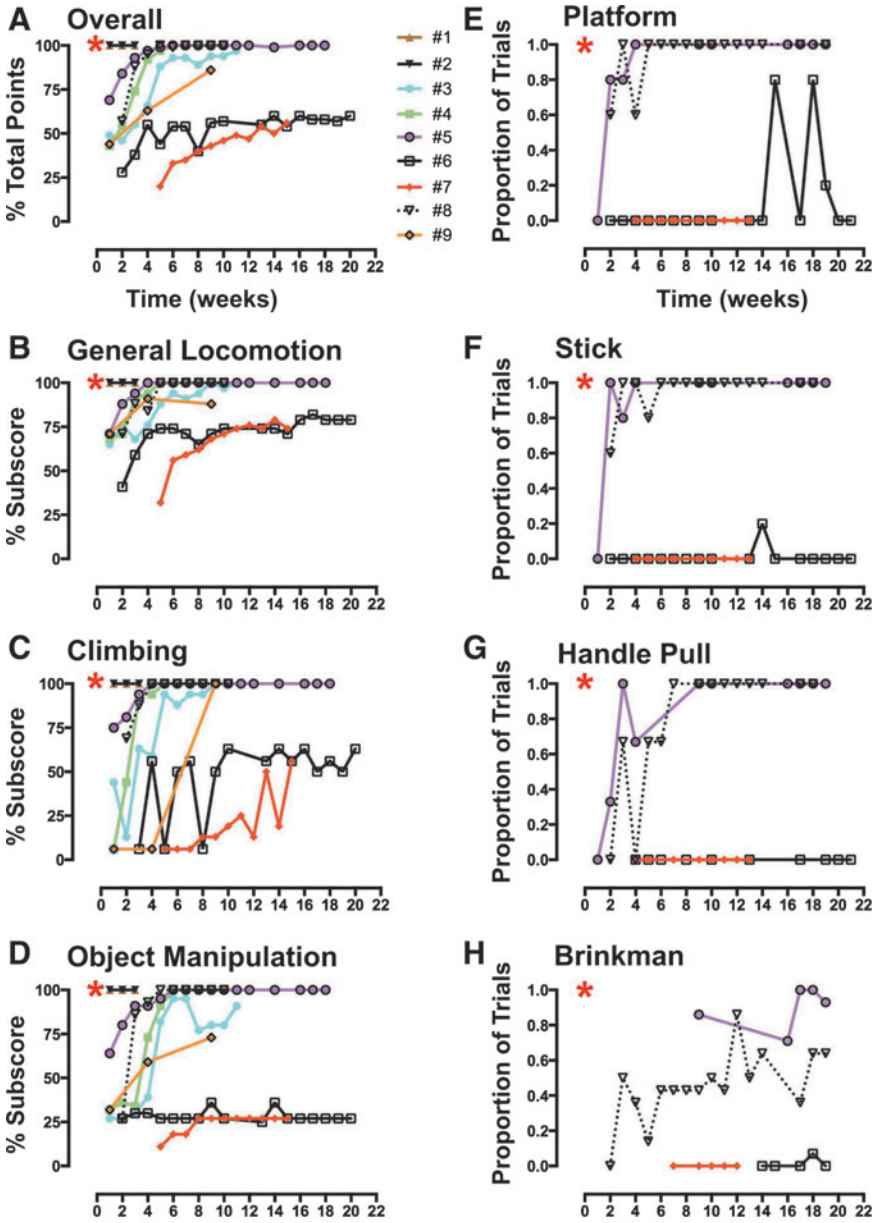

FIG. 6. Behavioral recovery during open field and chair testing shows that subjects exhibit a range of deficits early after injury that recover in some animals but persist in others. **(A)** Overall performance in the open field. Animals are awarded points (total = 72 points) for approximations to normal behavior on **(B)** general locomotion (limb use, placement, weight support, stepping and gait asymmetry; 34 points), **(C)** climbing (limb use during climbing, grip strength and retrieval of food items from cups at various heights; 16 points), and **(D)** object manipulation (posture, forelimb and finger movements while eating an apple or an orange, or during retrieval of food items from a Kong toy; 22 points). The overall score was derived by summing the subscore points for performance on all three activities (Table 3). A subset of animals (subjects #5, 6, 7, and 8) also were trained to perform four tasks with their impaired forelimb while seated in a standard primate-restraining chair; performance is shown as the proportion of trials where the reinforcer was successfully transferred to the mouth. These tasks involved retrieval of food rewards (e.g., grape, raisin, apple piece, etc.) from a platform **(E)**, from the top of a vertical post/stick **(F)**, from a 7-slot Brinkman board **(H)**, or for pulling and holding a U-shaped handle attached to springs of varying stiffness **(G)**. Two of the four subjects tested were able to successfully transfer food rewards to their mouth when performing all of these tasks (subjects #5 and #8). Sustained residual deficits in pincer grasp were evident on the Brinkman board task for all subjects. Red asterisk indicates pre-operative baseline performance.

side and trial also varied by location (side × location and trial × location: Wald chi-square = 20.532, $p < 0.0001$ and Wald chi-square = 12.337, $p = 0.006$, respectively).

Based on the observed interaction effects a *post hoc* chi-square test was performed at the second time-point (i.e., 4-5 weeks post-lesion) in the thoracic location. The proportion of responses allocated to the no response (count = 10), spinal (count = 1), and supraspinal (count = 13) response category were significantly different (chi-square = 9.750, $p = 0.008$), indicating that the animals were particularly responsive to stimulations at the thoracic site at the intermediate time-point. Overall, these data suggest that: 1) the probability of a response changed within session, perhaps

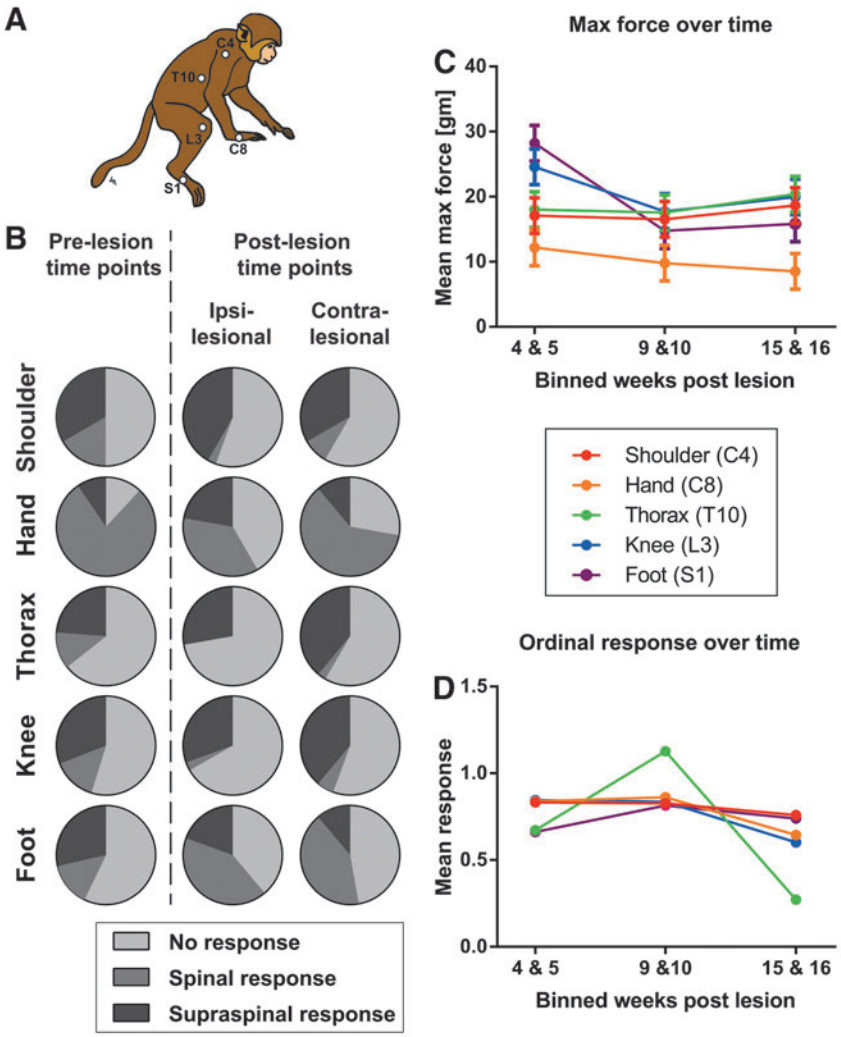

FIG. 7. Results of the Von Frey Hair (VFH) sensory assessment. **(A)** Schematic drawing of the monkey with the stimulation sites indicated as white dots. **(B)** Response category distribution for the different VFH stimulation sites pre-injury ($n=3$) and post–spinal cord injury ($n=4$). Response rate (either segmental or supraspinal) was about 50% with the hand stimulation producing the most responses. No wince or vocalizations were ever recorded; thus, supraspinal responses included only orientation or activity arrest. False alarm trials almost never produced a response. **(C, D)** The graphs show the interaction effect between the binned weeks post-lesion (x-axis) and the color-coded locations with the mean maximum force (C) and the mean response (D) on the y-axis (0 = no response, 1 = spinal responses and 2 = supraspinal responses). The thoracic location (D) shows an increase in supraspinal responses at the 9–10 weeks post-lesion followed by a decrease at the latest time-point. Data are averaged across all subjects tested ($n=4$). Means represent estimated marginal means ± standard error of the mean.

indicative of habituation; 2) there were differences across sites in responsivity; and 3) responses to stimulation were relatively constant across post-operative testing, except that supraspinal responses to thoracic stimulation appeared to be enhanced in the intermediate post-operative period. Together, these results suggest that the von Frey testing provided a means of evaluating potential changes in sensation as reflected by tactile sensitivity, but that the unilateral cervical lesion did not produce dramatic impact on somatic sensation as indicated by this test.

Assessment of tone

The same four subjects tested in the primate chair had muscle tone assessed by the experimenter at the beginning of each chairing session using the modified Ashworth scale (Fig. 8). Statistical analysis using generalized estimating equations revealed an effect of time on the Ashworth response (main effect of time: Wald chi-square = 17.657, $p=0.001$, error bars indicate SEM; $n=4$), indicating that the group displayed a gradual, slight increase in tone over time after the injury.

Multivariate analysis

We performed a series of PCAs on the aggregate mechanical, anatomical, and behavioral dataset to determine whether the NHP model showed a syndromic pattern similar to that seen in our rat studies,[14,26] and to derive a composite integrated measure suitable for evaluating therapies. Figure 9 shows the results of the multivariate PCA. This analysis included exercise cage data and biomechanical and lesion parameters for subjects that had lesions ($n=7$), but did not include primate chair data since only four of animals were tested on those tasks. This allowed for a PCA without the need to impute missing values. PCA resulted in two principal components (PC) that together accounted for >65.08% of the total variance in the dataset (PC2 not shown). PC1 (42.1% of variance; Fig. 9A) provides

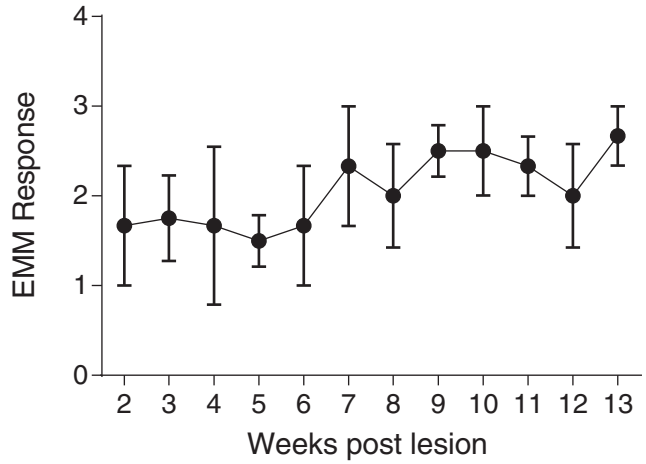

FIG. 8. Results of the modified Ashworth scoring. Using the modified Ashworth scoring system (see Methods for details), there was a significant increase in tone observed over the post-contusion survival period across all subjects tested ($n=4$; error bars represent standard error of the mean). EMM, estimated marginal means.

a measure of integrated biomechanics, lesion size, and neurological outcomes. Qualitatively, it is strikingly similar to the PC we observed in the rat,[14] with the highest PC loadings showing tight relationships between peak force, lesion volume, and exercise cage performance. Figure 9B shows the overall effect of injury (SCI), compared with baseline on PC1 for the group. We suggest that these kinds of derived syndromic measures will be useful for hypothesis testing when evaluating therapeutics in this model.

As a practical matter, we also were interested in the predictive value of the impact biomechanical parameters for neurological outcomes early in recovery. We looked at this in two ways. First, we performed a PCA of the dataset encompassing early (3 week exercise cage) behavioral outcomes, biomechanical and histological variables. This analysis (Fig. 10A) shows again a tight clustering of variance (42.1%) accounted for by the relationship between peak force (0.94), lesion volume (-0.96), white matter sparing (0.90), and total exercise cage performance (0.84). Second, as a comparison to this analysis, we looked at the univariate Pearson correlation coefficient between peak force and exercise cage performance at the 2 week time-point and included all nine animals in the analysis (Fig. 10B). This more conventional analysis showed a high correlation ($r>0.87$) between these two variables, and suggests that at the time of surgery, when the biomechanical readouts are available for each injury, we can well predict the neurological status of each animal at 2 weeks. This will allow prior stratification of treatment groups receiving, for example, cellular transplant therapies at 2-3 weeks after injury. In addition, examination of the full correlation matrix used to generate the PCAs showed that peak force was predictive of both behavioral outcomes (including chair performance) and anatomical outcomes in the entire set of animals evaluated (Fig. 5). Thus, in the NHP as observed in our rat models, with either conventional or syndromic analysis, there is a clear relationship between impact parameters, histology, and behavior.

CST projections above, at, and below the lesion epicenter

Subjects #5 and #6 had extensive BDA labeling of nearly the entire motor cortex in both the forelimb and hindlimb regions, densely labeling the CST in the upper cervical region (supplementary Fig. S3; see online supplementary material at www.liebertpub.com). The distribution of the CST to areas 5.2 mm above, at, and 5.2 mm below the lesion epicenter for both subjects is shown in Figures 11 and 12. For each BDA-labeled spinal cord region shown, a matching EC-stained section also is displayed to

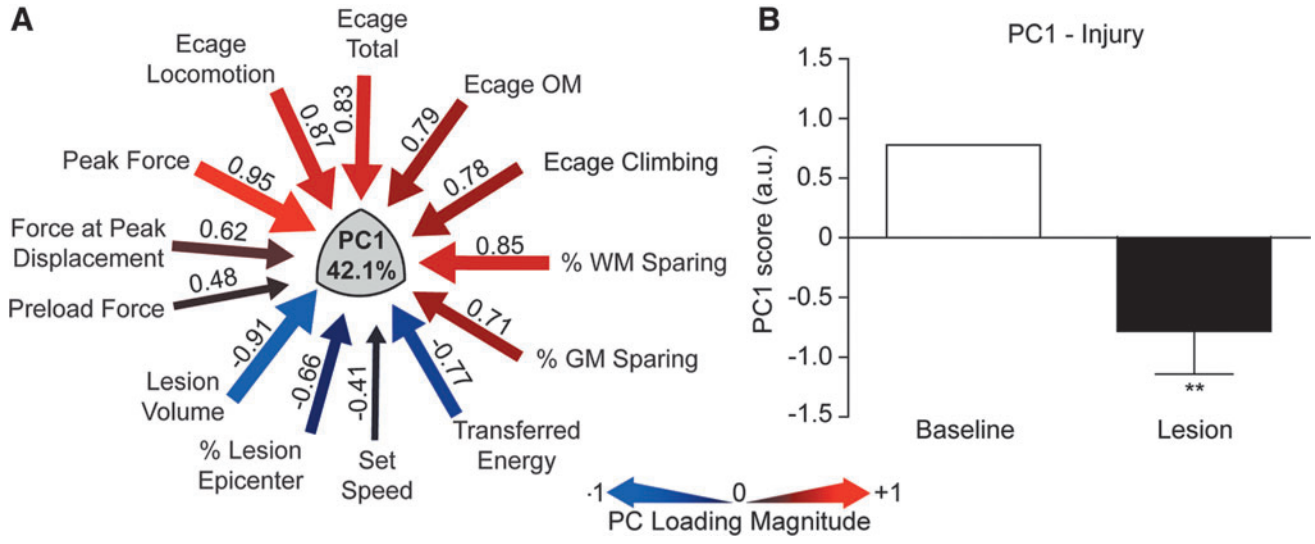

FIG. 9. The results of a principal components analysis (PCA) evaluating the relationship between all biomechanical, histological, and open field behavioral outcomes for subjects with contusion lesions ($n=7$). Note that chair task performance was excluded from this analysis because only a subset of the animals was trained and tested on these tasks. **(A)** PCA revealed a principal component (PC1) that accounted for 42.1% of the variance in the dataset, and shows high loadings for peak force (0.95), % white matter sparing (0.85), and total open field score (0.83), which are inversely correlated to the lesion volume (–0.91). **(B)** Using the PCA-derived composite scores for each monkey, grouped as either baseline (pre-injury) or lesion (post-injury), a general linear model of these group PC scores for PC1 was tested. PC1 was significantly predicted by the injury, compared with baseline values (**$p<0.001$).

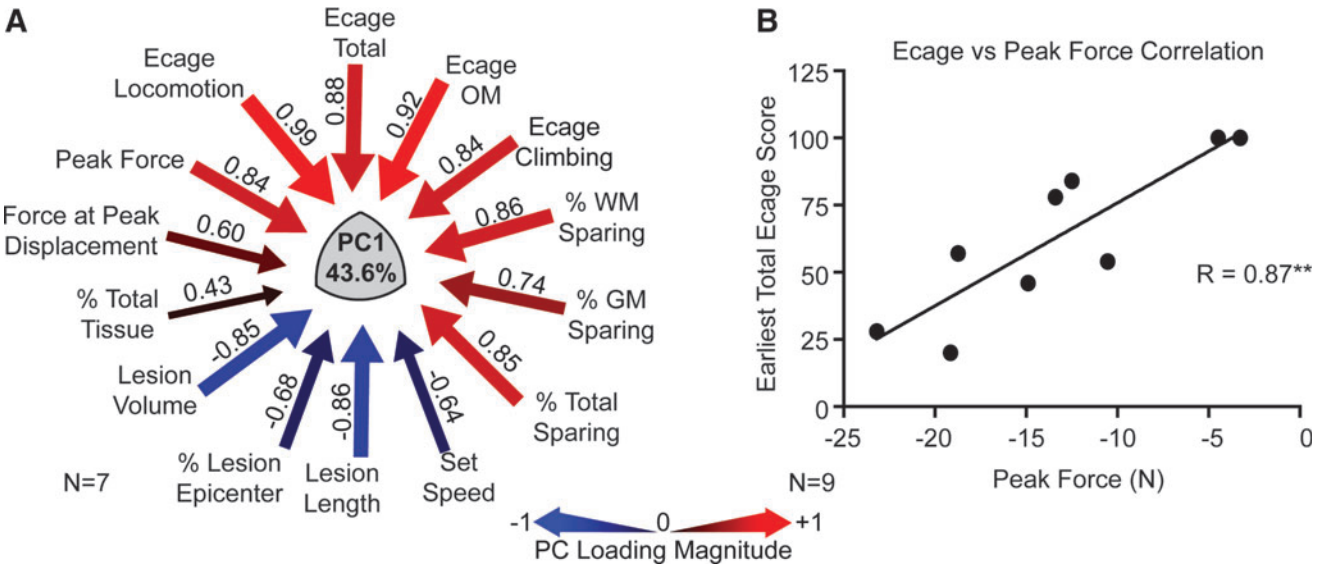

FIG. 10. Assessment of the association between early behavioral performance (first 3 weeks), biomechanical variables, and terminal histology. **(A)** The principal components analysis (PCA) evaluating the relationship between all biomechanical, histological, and early recovery variables yielded a first principle component accounting for 43.6% of the variance, which was very similar to that determined for the entire recovery period (Fig. 9). The same high loadings on PC1 for peak force, exercise cage performance, and % sparing at the lesion site were revealed in this analysis. This indicates the high degree of association between the biomechanical variables obtained at the time of surgery and early recovery (as well as anatomical outcomes). **(B)** A univariate Pearson correlational analysis showed a similar strong correlation between contusion peak force and function at 2 weeks. Both of these analyses suggest that the biomechanical variables, which are available at the time of surgery, can well predict the short and long term recovery, as well as the anatomical outcomes, making them useful for counterbalancing groups in treatment trials.

demonstrate the extent of demyelination due to the lesion, the boundaries of the lesion, and the associated regions of tract degeneration. The lesion in subject #5 (Fig. 11) spared the lateral-most aspects of the CST. Above the lesion (C6; Fig. 11 A-E), CST projections were observed in both white and gray matter regions ipsilateral to the lesion. There was dense labeling of the dorsolateral CST in the lateral funiculus and extensive distribution to the base of the dorsal horn, the intermediate gray and the ventral horn (Fig. 11 B, 11C). In the region of the central canal (Fig. 11 D), fibers could be seen crossing to the opposite side of the cord. Consistent with previous observations,[11] a small number of BDA-labeled fibers descending ipsilateral to the cortical labeling were also observed in the dorsolateral and ventromedial funiculi (data not shown).

At the lesion epicenter (C7-8; Fig. 11F-K), CST projections were evident in the lateral aspect of the main tract (Fig. 11F, 11G) in the spared rim of tissue (see EC-stained section for lesion boundary). Some fibers formed retraction-bulbs at the lesion margin (Fig. 11H), and no fiber labeling was evident in the lesion area (Fig. 11F, 11G; see EC-stained section for the lesion margins) or crossing at the central canal (Fig. 11I). However, on the side contralateral to the lesion, CST projections appeared to be conserved in both the dorsolateral (Fig. 11J) and ventromedial (Fig. 11K) CST. Below the lesion (C7-8, 5.2 mm caudal to the lesion epicenter; Fig. 11L-Q), CST projections exhibited a similar pattern of distribution as that observed above the lesion, although the density was reduced. BDA-labeled fibers traveling in the lateral funiculus ipsilateral to the lesion appeared to stream from lateral to medial (Fig. 11Q, arrows) across the demyelinated region previously occupied by the CST axons interrupted by the lesion (Fig. 11; see matching EC-stained section). These axons distributed to the same regions of the gray matter as the normal input, that is, the base of the dorsal horn, the intermediate gray (Fig. 11L), the ventral horn (Fig. 11M, 11N), and crossing the midline at the central canal (Fig. 11P). A Nissl counterstained section below the lesion demonstrates CST terminal projections to motor neurons (MN) in the ventral horn (Fig. 11O). CST projections in the dorsolateral and ventromedial CST contralateral to the lesion also were found below the lesion (data not shown).

In contrast, the lesion in subject #6 was larger at the epicenter as well as rostro-caudally (Fig. 4), and the respective CST labeling in the lateral funiculus and the gray matter distribution shown in Figure 12 was far less extensive. Notably, the degree of tract labeling at the high cervical level (C3) between the two cases is similar (supplementary Fig. S3), the labeling at 5.2 mm above the lesion in subject #6 (C6-7) is more sparse than in subject #5 even though this section is equidistant from the lesion epicenter, although, the same regions in the gray have axonal arbors. At the lesion epicenter (C6-7; Fig. 11 F-K) and below (C8; Fig. 11 L-Q), few fibers are labeled in the lateral funiculus, and few axonal arborizations can be seen below the lesion in the gray. Indeed, the density of CST projections in the gray below a spinal lesion has been shown to correlate with the degree of functional recovery,[11] and these two cases showed good recovery (subject #5) and poor recovery (subject #6), respectively.

Discussion

Here, and in the companion article[17] we describe the development of a unilateral cervical contusion injury device and its use in the macaque monkey. The device and procedure allows the production of graded contusion lesions and varying degrees of recovery depending upon pre-set impact parameters. As we progressed through this initial series, we incorporated new protocols and the use of pre-operative MRI to increase the predictability of the outcomes by matching impact protocols to individual features

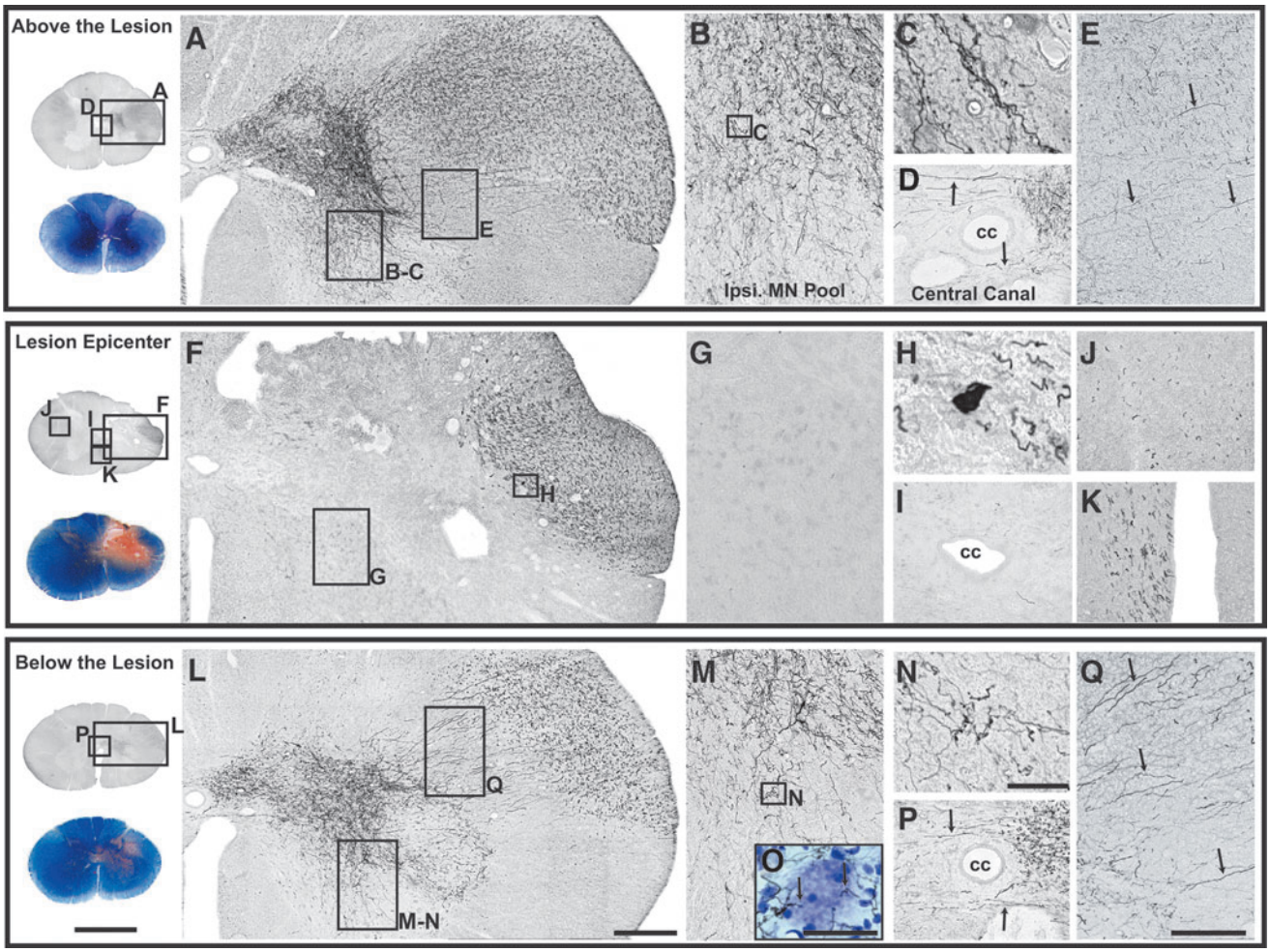

FIG. 11. Corticospinal tract (CST) projections after a right C7 spinal cord contusion injury and anterograde labeling of the left primary motor cortex using biotinylated dextran amine (BDA; subject #5). Sections above **(A-E),** at **(F-K),** and below **(L-Q)** the lesion are shown. An adjacent orientation section stained with eriochrome cyanine (EC) and neutral red is shown at the far left of each panel and reveals the lesion and gray and white matter sparing. At C6 and 5.2 mm above the lesion, a high density of labeled CST fibers (A) were observed in the lateral funiculus coursing medially (E, small arrows) to distribute to the base of the dorsal horn, the intermediate zone, the ventral horn (B-C), and central canal area (D). CST projections also were found in the dorsolateral and ventromedial tracts contralaterally (data not shown). At the lesion epicenter (C6-7), descending BDA-labeled fibers were only detected laterally (F), and were not observed to project into the gray matter (G) or crossing the central canal (I). Remaining CST projections at the lesion margin formed retraction bulbs (H). Contralateral to the lesion, descending fibers (ipsilateral to side of cortical labeling) were present in the dorsolateral (J) and ventromedial (K) CST. Below the lesion (at C7-C8, and 5.2 mm caudal to the lesion epicenter), remaining CST projections continued to descend in the lateral funiculus (L) and were observed to re-establish terminal distributions in the intermediate gray, ventral horn (M-O), and central canal (P) via streams of axons crossing the area where CST fibers had been interrupted by the lesion (Q, small arrows). This area of CST degeneration is devoid of myelin staining (note the pink area in dorsolateral funiculus in the EC-stained orientation section at far left) demarcating the degenerated CST below the lesion. BDA-labeled fibers in dorsolateral and ventromedial tracts were detected on the side contralateral to the lesion at all levels (data only shown for the lesion epicenter J, K). A Nissl counterstained section below the lesion demonstrates CST terminal projections to motor neurons in the ventral horn (O). Scale bar for orientation sections = 4 mm; scale bar in L = 400 μm and applies to A and F; scale bar in N = 50 μm and applies to C, H and O; scale bar in Q = 300 μm and applies to B, D, E, G, I, J, K, M, and P. Ipsi MN Pool, ipsilateral motor neuron pool; cc, central canal.

of each animal's spinal canal, spinal cord, and CSF space. Post-operative MRI provided confirmation of lesion placement, as well as information on lesion volume and extent. We produced a series of animals with lesions varying from small to large, were able to evaluate the relationships between impact parameters, lesion measures, and behavioral outcomes, and were able to confirm that these relationships were consistent with our previous studies in the rat.[7,14] Multiple univariate outcome measures are provided, as well as an integrated metric characterizing the multivariate cervical SCI syndrome. Impacts at the higher ranges of peak force produced highly lateralized and enduring deficits in multiple measures of forelimb and hand function, while lower energy impacts produced early paralysis followed by substantial recovery with enduring deficits in fine digital control (e.g., pincer grasp).

The device and protocol

The first model of contusion SCI was developed by Allen in 1911 and used a weight dropped from a calibrated height.[27] This

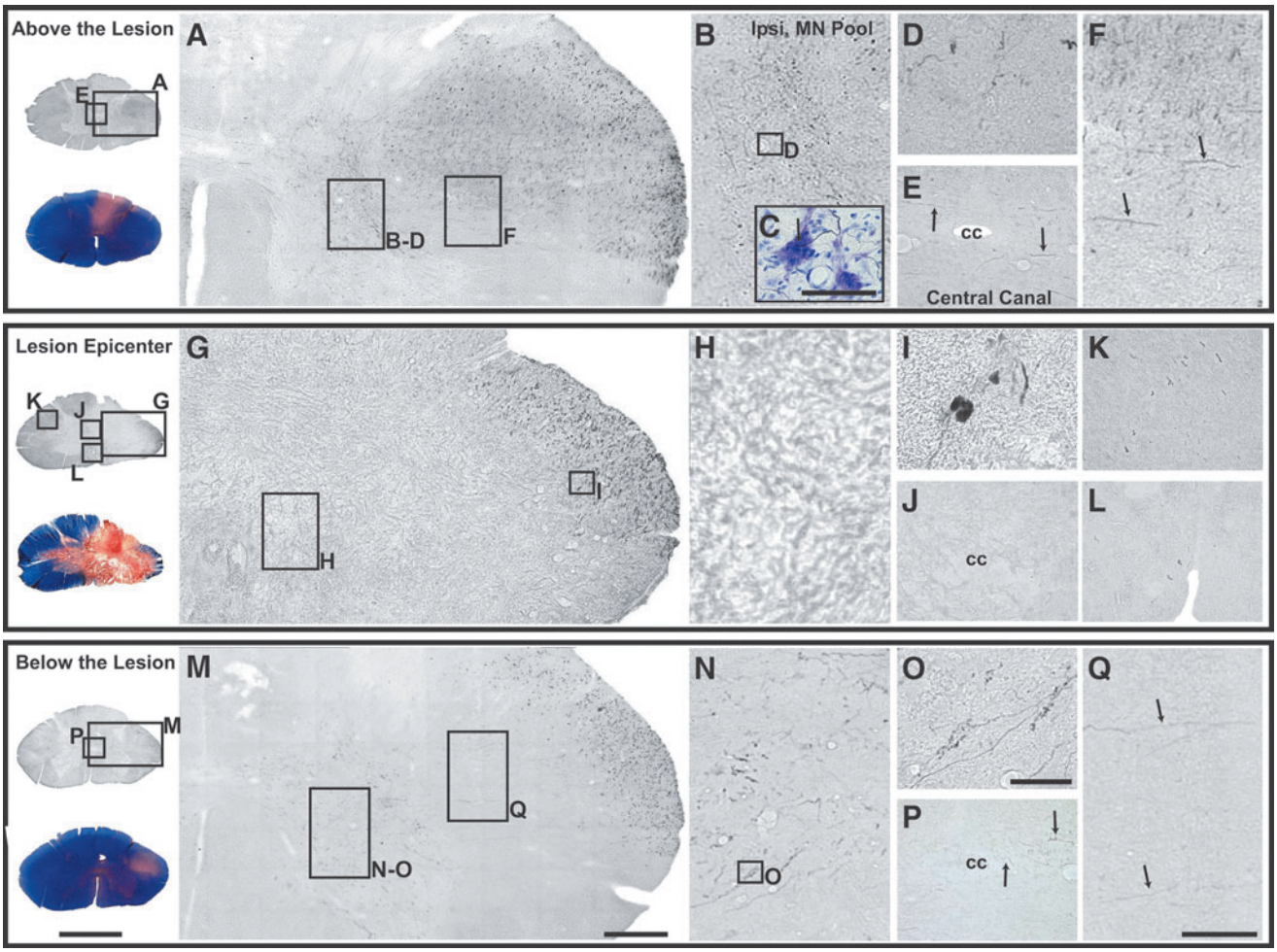

FIG. 12. Corticospinal tract (CST) projections from an animal with a more severe SCI (subject #6). Sections were selected at the lesion epicenter and at equal distances as those shown in Figure 11 (at C6-C7, 5.2 mm rostral, and at C8, 5.2 mm caudal to the lesion epicenter). Regions above **(A-F),** at **(G-L),** and below **(M-Q)** the lesion are shown. Eriochrome cyanine–stained orientation sections also are presented on the far left to demonstrate the areas of demyelination and the lesion boundaries. Above the lesion, although to a lesser extent than in the previous case, CST projections can be seen in the lateral funiculus (A), ventral horn (B-D), central canal area (E), and dorsolateral funiculus (F). The Nissl counterstained inset shown in (C) was taken from an adjacent section at that same level and region as in (D) and shows terminal arborizations in the vicinity of motor neurons. At the lesion epicenter, (C6-7), ipsilateral to the lesion (G-H), biotinylated dextran amine–labeled fibers were only seen laterally in the dorsal lateral funiculus, and those close to the lesion margin exhibited retraction-bulbs (I). Contralateral to the lesion, CST fibers were observed in the dorsolateral (K) tract but almost no fibers were observed in ventromedial (L) tract, likely due to the lesion extending across the midline. Below the lesion (C8), few CST fibers were observed to project out of the main tract and course medially (Q, small arrows) to terminate in the intermediate gray, ventral horn (M-O), and central canal area (P). Note the differences in density of CST fibers between subjects #5 and #6 are likely due to variations in lesion severity as the tract labeling seemed comparable between the two cases (supplementary Fig. S3). Scale bar for orientation sections = 4 mm; scale bar in M = 400 μm and applies to A and G; scale bar in O = 50 μm and applies to C, D, and I; scale bar in Q = 300 μm and applies to B, E, F, H, J-L, N, and P.

same method was used in studies in large animal models of SCI in the 1970s and 1980s, including NHPs.[24,28] Studies in cats were used to develop methylprednisolone as a therapy and implemented either weight drop techniques,[29,30] or a static compression model.[31,32] The evolution of SCI contusion injuries included a weight-drop device with computer-generated impact parameters (MASCIS),[33,34] a waveform-controlled electrical impactor (the OSU device)[22,35–37] and most recently, the Infinite Horizons (IH) device.[38] Our prior rat unilateral cervical contusion lesions were produced by the MASCIS device (free-fall),[7] and more recently by the IH device.[14,23] In order to provide the necessary range and force to scale up these models to the macaque monkey, we chose to use a friction-free, electromagnetic linear actuator (Bose ElectroForce) that was developed for materials testing, has a wide range of programmable displacement, force, and feedback modes, and provides independent control of the magnitude and rate of impact.[17] A similar device also has been used to develop models of different spinal cord injury mechanisms in rats[39,40] and in biomechanical studies of spinal cord tissue.[41] Finite element analysis and testing on surrogate cord material provided estimates for scaling up the impactor size, displacement, and force ranges from our prior rat work to the size of the monkey cord,[17] and the surrogate cord we developed allowed us to pre-test our displacement waveforms to predict resultant peak force prior to each impact.

MRI for impact planning and detection of lesions

MRI allowed for the collection of pre-operative measurements on the size of the spinal cord and the size of the CSF compartment at the impact site at spinal level C6-C7. As we confirmed with our first two subjects, the large CSF space in the monkey allowed for movement of the cord during impact. Using this information, we tailored each impact by exerting a vertical pre-loading force onto the exposed dura to temporarily displace the CSF and trap the spinal cord against the floor of the vertebral canal. Comparison of the MRI signal to post-mortem histological analysis showed that the magnetic resonance hyperintense signal underestimated the size of the lesion as determined by histology. This is likely due to limitations in the acquired MRI sequences to detect injured regions of the cord parenchyma that maintained cellular content. Regardless of this limitation, the applicability of such technology, coupled with more refined imaging protocols, could have strong clinical implications for designing treatment regimens specific to each case/lesion, and we have used magnetic resonance imaging–based lesion volume estimates to predict the volume of cells needed to fill cavities (data not shown). In this regard, the move from a 1.5T to a 3T scanner provided clear increases in signal to noise and more distinct boundaries of the T2 hyperintense regions.

Relationship of impact parameters to lesion characteristics

The impact parameters were chosen in an attempt to produce contusion lesions in NHPs similar to those we had produced in the rat.[7,14,23] We aimed to produce a rapid (20 msec) deformation of the cord to approximate a rapid fracture dislocation. Testing and simulations[17] provided a displacement range that would produce forces sufficient to produce large lateralized lesions. We started off with low displacement and moved up as we progressed in the series, producing a variety of injuries as intended. We then were able to examine the relationship between various impact parameters and the resultant lesion using correlational and multivariate analyses. We chose to use a displacement-controlled protocol modeled after our earlier work with the OSU device,[22,37] which used a pre-set load of 3000 dynes to displace CSF and provide a stable starting point for the displacement.[42] Procedures necessary to establish a stable starting point also were required in the present study (Fig. 1). In our experience with multiple contusion injury devices, this protocol seemed to produce the most consistent injuries,[37,43,44] and since the analysis from Romanowski and colleagues[45] indicated we needed to displace CSF, it had the advantage of starting from a static position (rather than dropping a weight or, as with the IH device, backing off away from the cord prior to impact). The drawback of our approach is that starting from zero velocity requires the impactor to accelerate rapidly in order to reach desired velocities. Thus, the frictionless, high-speed, controllable actuator from Bose was the only available unit that could provide up to 1 m/sec impact velocity over short distance (2-4 mm) starting from rest.

Our analysis showed that the peak force obtained during the $\sim$20 msec impact was highly predictive of lesion volume, and multivariate analysis showed that peak force and force at maximum displacement tracked well with lesion descriptors and neurological outcomes. Given the strong correlation between force and lesion volume, it might be useful to try to control force in this model, but that would leave displacement uncontrolled. However, using force feedback to control a high dynamic rate event in compliant tissue risks instability in the system. In addition, as discussed in the companion article[17] inertial compensation must be applied to determine an accurate measure of impact force applied to the spinal cord and may not be achievable at the high loading rates required to simulate traumatic injury.

Many other models of SCI have used different parameters that vary the speed and dwell time of the impact, or use static compression to achieve injury. A discussion of the mechanisms of injury in these different models is beyond the scope of this paper, but it is likely that slower, compressive injuries have a more ischemic nature than rapid injuries, and could produce less axon breakage but more demyelination.[46–48] Slower compression injuries with longer dwell times or combined rapid impact with residual compression may all be useful in modeling different kinds of SCI in large animal models.[49,50] One advantage to the system we have employed is that it can be programmed to provide essentially any pattern of displacement or force over short or long intervals, and so it could be adapted to study these other aspects of SCI. Its main limitation is that it cannot achieve the very rapid speeds (many meters per second) that may be encountered in high speed vehicular or projectile impacts.

The lesions produced in our study, similar to those in our rat models, produce both gray and white matter injuries, and these extend rostral and caudal to the lesion epicenter. Thus, neurological deficits are produced by a combination of gray and white matter damage, with gray matter damage affecting lower motor neurons and circuits involved in upper extremity function and damage to white matter tracts affecting connections from rostral CNS regions to those circuits and to autonomic and hindlimb locomotor centers in the caudal spinal cord. Separating the effects of gray and white matter damage on neurological function in this kind of model is difficult, but it is clear that the larger the lesion, the more local neuronal damage and the fewer connections available to drive them. We chose to make impact lesions centered on the C6-C7 spinal cord segment (C5 vertebral level). Since the intrinsic muscles of the hand are innervated by levels caudal to C7, we reasoned that as lesions became larger, they could affect hand function in two ways—by impinging on more caudal motoneuron pools and circuits involved in digital function, and by denervating the caudal neuronal circuits involved in hand function (upper motor neuron lesions).

Our behavioral outcomes were meant to capture functional deficits in both hand and proximal forelimb function. Although a discussion of the details of recovery with respect to the descending pathways and intrinsic circuits is beyond the present data, the primate provides a particularly rich opportunity to examine these relationships in detail, and we intend that the present model be used for just such an analysis. For the present study, we can simply say that we found that lesions extending to the most lateral aspects of the white matter produced the most enduring deficits in hand function, even though most of the motoneuron pools involved were presumably spared. Thus, treatments that protect or enhance reconnections could result in incremental improvements in distal limb and hand function in this model. The CST sparing shown in Figures 11 and 12 is an example of how this model may eventually relate spared, sprouted, or reconnected axons to recovery of function in the primate. With respect to gray matter lesions, since the technology is available to instrument our animals with chronic indwelling EMG electrodes,[11,13] this model would seem to provide a wonderful opportunity to label muscles to evaluate the role of partial sparing of motor neuron pools in the recovery of function.

Lesions and behavioral outcomes

Our group has reported in some detail the deficits and patterns of recovery after C7 hemisection in the monkey.[11–13] The present study used the same neurological outcome measures, including the

use of the open field exercise cage scoring system. In general, we found that contusion lesions produced similar patterns of initial deficit and recoveries, with the exception that partial contusion lesions recover functional motor skills better than animals with complete hemisection. The largest lesions in this study, however, resulted in recoveries that were comparable to the recoveries seen after complete hemisection. It should be noted that even NHPs with over-complete hemisections can show recovery of considerable hand function,[12] so that lesion size *per se* is not always a strict predictor of outcomes. Almost all of the animals in this study with smaller lesions were able to score high marks in the open field and even in the chair tasks after a substantial recovery period. However, there remained motor deficits on the Brinkman board task, which requires pincer grasp. Others, who have studied recovery after partial lesion of the CST, have found similar recoveries, with deficits remaining only in fine digital control.[51–56]

As in the rat, unilateral cervical contusion injuries in the monkey produced less deficit in the ipsilateral hindlimb than the forelimb. In the rat, these deficits recover quite rapidly,[14,57] but a residual deficit can sometimes be seen using gait analysis.[7] In our prior work with complete spinal hemisections in the macaque, hindlimb deficits were more apparent but variable, with some animals showing severe deficits in open field and treadmill locomotion and others showing little. Interestingly, a subset of NHPs with complete spinal cord hemisections showed either forelimb or hindlimb locomotor dysfunction, but not both. The extensive crossing of multiple descending pathways related to locomotion (e.g., reticulo-spinal, serotonergic, and even CST[19] is likely to be responsible for the recovery of locomotor function in both species). Further, all of our contusion injuries spared at least a small number of CST fibers and the CST contralateral to the lesion, which may also contribute to better recovery.

Syndromics and therapeutic testing

In order to capture as much information as possible on recovery after hemisections and hemicontusions, we have employed multiple anatomical and behavioral outcome measures over an extended post-injury period.[11,13] Multivariate analyses are useful in assessing how those outcomes co-vary and how they are related to mechanical parameters of the injury, but they also may provide some insight into the nature of the recovery process. Principal component analysis can yield more tractable measures of multivariate high density data,[58] and is applicable to multiple measures of SCI outcomes.[11,18,23] In the present study, PCA revealed a principal component, PC1, that encompassed relationships between injury parameters, lesion characteristics, and neurological outcomes that accounted for a large portion of the shared variance across measures. Further, this component was quite similar to that produced by a similar analysis of somewhat different outcome measures in the rat unilateral cervical contusion injury.[14,23] This suggests that there is a rather global syndrome of cervical SCI that is reflected to varying degrees in different outcome measures, reflected in their loadings onto PC1 (Fig. 9). It also suggests that this syndrome may be translatable across species.[18]

Finally, since some outcome measures are highly linked to this underlying pattern of dysfunction and recovery, it may be that an accurate picture of recoveries and treatments could be obtained by choosing outcomes that load especially highly on the PC metric(s). However, it should be noted that the syndromic metrics in this study are generated by a lot of variables but ignore some potentially important underlying biological features of injury and repair, such as sprouting and regeneration,[11] immune responses, genetic predispositions, etc. Thus, it may be best to continue to increase rather than cherry-pick outcomes in our model. Particularly given the huge time commitment, expense, and use of highly-valued animals, we would like to choose more data, rather than less. Nevertheless, when decisions about time and resources have to be made, this analytic approach may be of value.

Limitations of the model

These contusion lesions are intended to model human cervical cord lesions caused by fracture dislocation. The less severe lesions also resemble central cord syndromes observed in humans with less extensive injury. The appearance of the lesions on MRI and in post-mortem histology resemble clinical observations,[59–61] with the exception that these lesions are, of course, lateralized. Brown-Sequard syndrome[62,63] describes cases of unilateral human injury, and our NHPs exhibit similar neurological signs to this relatively rare human syndrome. Kalsi-Ryan and colleagues recently charted the course of upper extremity recovery in 53 cervical SCI patients over one year.[64] The recovery curves shown in that paper are notable for the substantial recovery in almost all of the measures used, no matter the Abbreviated Injury Scale (AIS) grade. The recovery curves are qualitatively quite similar to those of our study.

At first glance, perhaps the most like our two end-point groups are AIS C and D (although animals with the most severe lesions were densely plegic for several days after injury on the right side, and might be considered to be ''unilateral AIS B,'' with the Cs having a considerable residual deficit, and the Ds having the most return of function with small enduring deficits in digital dexterity). The proportion of AIS C and D cervical injured patients in the small sample of the Kalsi-Ryan and colleagues' study was 70%. In the whole human SCI population, it is estimated that about $\sim$76% of cervical injuries are incomplete, which represent $\sim$45% of all SCI cases, so this represents a considerable number of patients.[65] So even with the limitations of the model imposed by animal care and practical issues, it is still clinically relevant to a large population. Questions of the contribution of the (mostly) intact contralateral side of the cord to recovery, however, remain.

The chief advantage of this model is that it recapitulates the mechanism of human SCI in an animal species that most closely approaches the human spinal cord in size and function. The chief drawback of the model is that it is incomplete: more than half the spinal cord is spared, potentially complicating interpretation of functional and anatomical outcomes because spared systems contribute extensively to recovery. Thus, one could argue that the chief value of the model is in scaling potential human interventions to a system most similar to humans, and in assessing safety on the background of a nervous system resembling humans. But the model may not be the best system for establishing efficacy, given the broad contribution of spared systems to functional recovery. However, if an experimental intervention tested in this primate model does indeed enhance recovery beyond the spontaneous, $\sim$50% improvement observed in animals with more extensive lesions, then one could reliably predict potential benefit in a human trial. In such a case, this model could indeed be highly significant in predicting potential clinical success. We are unable to perform complete spinal cord lesions in non-human primates because of the difficulty of caring for monkeys under circumstances wherein several-time daily bowel and bladder care would be required, and adequate comfort of monkeys would be unpredictable; in the present partial lesion model, monkeys retain bowel and bladder function and are generally readily mobile and capable of self care within days. Moreover,

we have not detected apparent persistent pain in monkeys with this type of lesion, expressed as self-injurious behavior or discomfort beyond the immediate post-operative period, nor do we see evidence of significant allodynia in the von Frey testing.

Based on the preceding discussion, some candidate translational therapies might merit testing in this model. These would include invasive cellular or gene therapies, or direct intra-spinal cord injections of substances (e.g., chondroitinase). Primate testing in a contusion model would both optimize method development for human translation, and determine whether the candidate interventions pose safety issues that are identifiable optimally in the primate. This would particularly be the case with therapies introduced into spinal cord regions rostral to the lesion, and in the cervical spinal cord especially. It is important to evaluate both positive and potentially negative effects of this procedure. Studies are currently underway in this model testing human stem cell therapies.[66]

Acknowledgments

This work was supported by grants from the Veterans Administration, the Craig H. Neilsen Foundation (grants 190557, 260965 and 313739), the NIH (NS042291, NS067092, and NS079030), and the Wings for Life Foundation.

Author Disclosure Statement

No competing financial interests exist.

References

1. Geissler, S.A., Schmidt, C.E., and Schallert, T. (2013). Rodent models and behavioral outcomes of cervical spinal cord injury. J. Spine Suppl. 4, 001.
2. Streijger, F., Beernink, T.M., Lee, J.H., Bhatnagar, T., Park, S., Kwon, B.K., and Tetzlaff, W. (2013). Characterization of a cervical spinal cord hemicontusion injury in mice using the infinite horizon impactor. J. Neurotrauma 30, 869–883.
3. Lee, J.H., Streijger, F., Tigchelaar, S., Maloon, M., Liu, J., Tetzlaff, W., and Kwon, B.K. (2012). A contusive model of unilateral cervical spinal cord injury using the infinite horizon impactor. J. Vis. Exp. 65, 3313.
4. Russell, C.M., Choo, A.M., Tetzlaff, W., Chung, T.E., and Oxland, T.R. (2012). Maximum principal strain correlates with spinal cord tissue damage in contusion and dislocation injuries in the rat cervical spine. J. Neurotrauma 29, 1574–1585.
5. Anderson, K.D., Sharp, K.G., and Steward, O. (2009). Bilateral cervical contusion spinal cord injury in rats. Exp. Neurol. 220, 9–22.
6. Dunham, K.A., Siriphorn, A., Chompoopong, S., and Floyd, C.L. (2010). Characterization of a graded cervical hemicontusion spinal cord injury model in adult male rats. J. Neurotrauma 27, 2091–2106.
7. Gensel, J.C., Tovar, C.A., Hamers, F.P., Deibert, R.J., Beattie, M.S., and Bresnahan, J.C. (2006). Behavioral and histological characterization of unilateral cervical spinal cord contusion injury in rats. J. Neurotrauma 23, 36–54.
8. Tator, C.H. (2006). Review of treatment trials in human spinal cord injury: issues, difficulties, and recommendations. Neurosurgery 59, 957–982.
9. Courtine, G., Bunge, M.B., Fawcett, J.W., Grossman, R.G., Kaas, J.H., Lemon, R., Maier, I., Martin, J., Nudo, R.J., Ramon-Cueto, A., Rouiller, E.M., Schnell, L., Wannier, T., Schwab, M.E., and Edgerton, V.R. (2007). Can experiments in nonhuman primates expedite the translation of treatments for spinal cord injury in humans? Nat. Med. 13, 561–566.
10. Kwon, B.K., Ghag, A., Reichl, L., Dvorak, M.F., Illes, J., and Tetzlaff, W. (2012). Opinions on the preclinical evaluation of novel therapies for spinal cord injury: a comparison between researchers and spinal cord-injured individuals. J. Neurotrauma 29, 2367–2374.
11. Rosenzweig, E.S., Courtine, G., Jindrich, D.L., Brock, J.H., Ferguson, A.R., Strand, S.C., Nout, Y.S., Roy, R.R., Miller, D.M., Beattie, M.S., Havton, L.A., Bresnahan, J.C., Edgerton, V.R., and Tuszynski, M.H. (2010). Extensive spontaneous plasticity of corticospinal projections after primate spinal cord injury. Nat. Neurosci. 13, 1505–1510.
12. Nout, Y.S., Ferguson, A.R., Strand, S.C., Moseanko, R., Hawbecker, S., Zdunowski, S., Nielson, J.L., Roy, R.R., Zhong, H., Rosenzweig, E.S., Brock, J.H., Courtine, G., Edgerton, V.R., Tuszynski, M.H., Beattie, M.S., and Bresnahan, J.C. (2012). Methods for functional assessment after C7 spinal cord hemisection in the rhesus monkey. Neurorehabil. Neural Repair 26, 556–569.
13. Nout, Y.S., Rosenzweig, E.S., Brock, J.H., Strand, S.C., Moseanko, R., Hawbecker, S., Zdunowski, S., Nielson, J.L., Roy, R.R., Courtine, G., Ferguson, A.R., Edgerton, V.R., Beattie, M.S., Bresnahan, J.C., and Tuszynski, M.H. (2012). Animal models of neurologic disorders: a nonhuman primate model of spinal cord injury. Neurotherapeutics 9, 380–392.
14. Ferguson, A.R., Irvine, K.A., Gensel, J.C., Nielson, J.L., Lin, A., Ly, J., Segal, M.R., Ratan, R.R., Bresnahan, J.C., and Beattie, M.S. (2013). Derivation of multivariate syndromic outcome metrics for consistent testing across multiple models of cervical spinal cord injury in rats. PloS One 8, e59712.
15. Nout, Y.S., Mihai, G., Tovar, C.A., Schmalbrock, P., Bresnahan, J.C., and Beattie, M.S. (2009). Hypertonic saline attenuates cord swelling and edema in experimental spinal cord injury: a study utilizing magnetic resonance imaging. Crit. Care Med. 37, 2160–2166.
16. Mihai, G., Nout, Y.S., Tovar, C.A., Miller, B.A., Schmalbrock, P., Bresnahan, J.C., and Beattie, M.S. (2008). Longitudinal comparison of two severities of unilateral cervical spinal cord injury using magnetic resonance imaging in rats. J. Neurotrauma 25, 1–18.
17. Sparrey, C.J., Salegio, E.A., Camisa, W., Tam, H., Beattie, M.S., Bresnahan, J.C. (2015). Mechanical design and analysis of a unilateral servical spinal cord contusion injury model in nonhuman primates. J. Neurotrauma (in press).
18. Nielson, J.L., Haefeli, J., Salegio, E.A., Liu, A.W., Guandique, C.F., Stuck, E.D., Hawbecker, S., Moseanko, R., Strand, S.C., Zdunowski, S., Brock, J.H., Roy, R.R., Rosenzweig, E.S., Nout, Y.S., Courtine, G., Havton, L.A., Steward, O., Edgerton, V.R., Tuszynski, M.H., Beattie, M.S., Bresnahan, J.C., and Ferguson, A.R. (2014). Leveraging biomedical informatics for assessing plasticity and repair in primate spinal cord injury. Brain Res. 1619, 124–138.
19. Rosenzweig, E.S., Brock, J.H., Culbertson, M.D., Lu., P., Moseanko, R., Edgerton, V.R., Havton, L.A., and Tuszynski, M.H. (2009). Extensive spinal decussation and bilateral termination of cervical corticospinal projections in rhesus monkeys. J. Comp. Neurol. 513, 151–163.
20. Bohannon, R.W. and Smith, M.B. (1987). Interrater reliability of a modified Ashworth scale of muscle spasticity. Phys. Ther. 67, 206–207.
21. Salegio, E.A., Kells, A.P., Richardson, R.M., Hadaczek, P., Forsayeth, J., Bringas, J., Sardi, S.P., Passini, M.A., Shihabuddin, L.S., Cheng, S.H., Fiandaca, M.S., and Bankiewicz, K.S. (2010). Magnetic resonance imaging-guided delivery of adeno-associated virus type 2 to the primate brain for the treatment of lysosomal storage disorders. Hum. Gene Ther. 21, 1093–1103.
22. Bresnahan, J.C., Beattie, M.S., Todd, F.D. 3rd, and Noyes, D.H. (1987). A behavioral and anatomical analysis of spinal cord injury produced by a feedback-controlled impaction device. Exp. Neurol. 95, 548–570.
23. Irvine, K.A., Ferguson, A.R., Mitchell, K.D., Beattie, S.B., Lin, A., Stuck, E.D., Huie, J.R., Nielson, J.L., Talbott, J.F., Inoue, T., Beattie, M.S., and Bresnahan, J.C. (2014). The Irvine, Beatties, and Bresnahan (IBB) forelimb recovery scale: an assessment of reliability and validity. Front. Neurol. 5, 116.
24. Bresnahan, J.C., King, J.S., Martin, G.F., and Yashon, D. (1976). A neuroanatomical analysis of spinal cord injury in the rhesus monkey (Macaca mulatta). J. Neurol. Sci. 28, 521–542.
25. Lindsey, A.E., LoVerso, R.L., Tovar, C.A., Hill, C.E., Beattie, M.S., and Bresnahan, J.C. (2000). An analysis of changes in sensory thresholds to mild tactile and cold stimuli after experimental spinal cord injury in the rat. Neurorehabil. Neural Repair 14, 287–300.
26. Bresnahan, J.C., Behrmann, D.L., and Beattie, M.S. (1993). Anatomical and behavioral outcome after spinal cord contusion injury produced by a displacement controlled impact device. Restor. Neurol. Neurosci. 5, 76.
27. Allen, A.R. (1911). Surgery of experimental lesion of spinal cord equivalent to crush injury of fracture dislocation of spinal column: a preliminary report. JAMA. 57, 878–880.
28. Bresnahan, J.C. (1978). An electron-microscopic analysis of axonal alterations following blunt contusion of the spinal cord of the rhesus monkey (Macaca mulatta). J. Neurol. Sci. 37, 59–82.

29. Young, W., DeCrescito, V., Flamm, E.S., Blight, A.R., and Gruner, J.A. (1988). Pharmacological therapy of acute spinal cord injury: studies of high dose methylprednisolone and naloxone. Clin. Neurosurg. 34, 675–697.
30. Young, W. and Flamm, E.S. (1982). Effect of high-dose corticosteroid therapy on blood flow, evoked potentials, and extracellular calcium in experimental spinal injury. J. Neurosurg. 57, 667–673.
31. Hall, E.D. and Braughler, J.M. (1982). Effects of intravenous methylprednisolone on spinal cord lipid peroxidation and Na+ + K+)-ATPase activity. Dose-response analysis during 1st hour after contusion injury in the cat. J. Neurosurg. 57, 247–253.
32. Means, E.D., Anderson, D.K., Waters, T.R., and Kalaf, L. (1981). Effect of methylprednisolone in compression trauma to the feline spinal cord. J. Neurosurg. 55, 200–208.
33. Basso, D.M., Beattie, M.S., Bresnahan, J.C., Anderson, D.K., Faden, A.I., Gruner, J.A., Holford, T.R., Hsu, C.Y., Noble, L.J., Nockels, R., Perot, P.L., Salzman, S.K., and Young, W. (1996). MASCIS evaluation of open field locomotor scores: effects of experience and teamwork on reliability. Multicenter Animal Spinal Cord Injury Study. J. Neurotrauma 13, 343–359.
34. Young, W. (2009). MASCIS spinal cord contusion model. In: *Animal Models of Acute Neurological Injuries.* J. Chen, X.M. Xu, and Z. Xu (eds). Humana Press: New York, pps. 411–421.
35. Noyes, D.H. (1987). Electromechanical impactor for producing experimental spinal cord injury in animals. Med. Biol. Eng. Comput. 25, 335–340.
36. Somerson, S.K. and Stokes, B.T. (1987). Functional analysis of an electromechanical spinal cord injury device. Exp. Neurol. 96, 82–96.
37. Behrmann, D.L., Bresnahan, J.C., Beattie, M.S., and Shah, B.R. (1992). Spinal cord injury produced by consistent mechanical displacement of the cord in rats: behavioral and histologic analysis. J. Neurotrauma 9, 197–217.
38. Scheff, S.W., Rabchevsky, A.G., Fugaccia, I., Main, J.A., and Lumpp, J.E., Jr. (2003). Experimental modeling of spinal cord injury: characterization of a force-defined injury device. J. Neurotrauma 20, 179–193.
39. Choo, A.M., Liu, J., Lam, C.K., Dvorak, M., Tetzlaff, W., and Oxland, T.R. (2007). Contusion, dislocation, and distraction: primary hemorrhage and membrane permeability in distinct mechanisms of spinal cord injury. J. Neurosurg. Spine 6, 255–266.
40. Choo, A.M., Liu, J., Liu, Z., .Dvorak, M., Tetzlaff, W., and Oxland, T.R. (2009). Modeling spinal cord contusion, dislocation, and distraction: characterization of vertebral clamps, injury severities, and node of Ranvier deformations. J. Neurosci. Methods 181, 6–17.
41. Shetye, S.S., Troyer, K.L., Streijger, F., Lee, J.H., Kwon, B.K., Cripton, P.A., and Puttlitz, C.M. (2014). Nonlinear viscoelastic characterization of the porcine spinal cord. Acta. Biomater. 10, 792–797.
42. Stokes, B.T., Noyes, D.H., and Behrmann, D.L. (1992). An electromechanical spinal injury technique with dynamic sensitivity. J. Neurotrauma 9, 187–195.
43. Behrmann, D.L., Bresnahan, J.C., and Beattie, M.S. (1993). A comparison of YM-14673, U-50488H, and nalmefene after spinal cord injury in the rat. Exp. Neurol. 119, 258–267.
44. Behrmann, D.L., Bresnahan, J.C., and Beattie, M.S. (1994). Modeling of acute spinal cord injury in the rat: neuroprotection and enhanced recovery with methylprednisolone, U-74006F and YM-14673. Exp. Neurol. 126, 61–75.
45. Romanowski, K., Nout, Y.S., Beattie, M.S., Bresnahan, J.C., and Sparrey, C.J. (2011). *Interspecies Variation in Spinal Cord and Column Morphology and Its Affect on Cord Compression Mechanics.* Society for Neuroscience: Washington, D.C.
46. Sparrey, C.J., Choo, A.M., Liu, J., Tetzlaff, W., and Oxland, T.R. (2008). The distribution of tissue damage in the spinal cord is influenced by the contusion velocity. Spine 33, E812–E819.
47. Lam, C.J., Assinck, P., Liu, J., Tetzlaff, W., and Oxland, T.R. (2014). Impact depth and the interaction with impact speed affect the severity of contusion spinal cord injury in rats. J. Neurotrauma 31, 1985–1997.
48. Gledhill, R.F., Harrison, B.M., and McDonald, W.I. (1973). Demyelination and remyelination after acute spinal cord compression. Exp. Neurol. 38, 472–487.
49. Lee, J.H., Jones, C.F., Okon, E.B., Anderson, L., Tigchelaar, S., Kooner, P., Godbey, T., Chua, B., Gray, G., Hildebrandt, R., Cripton, P., Tetzlaff, W., and Kwon, B.K. (2013). A novel porcine model of traumatic thoracic spinal cord injury. J. Neurotrauma 30, 142–159.
50. Jones, C.F., Kwon, B.K., and Cripton, P.A. (2012). Mechanical indicators of injury severity are decreased with increased thecal sac dimension in a bench-top model of contusion type spinal cord injury. J. Biomech. 45, 1003–1010.
51. Nishimura, Y., Morichika, Y., and Isa, T. (2009). A subcortical oscillatory network contributes to recovery of hand dexterity after spinal cord injury. Brain 132, 709–721.
52. Nishimura, Y., Onoe, H., Morichika, Y., Perfiliev, S., Tsukada, H., and Isa, T. (2007). Time-dependent central compensatory mechanisms of finger dexterity after spinal cord injury. Science 318, 1150–1155.
53. Alstermark, B. and Isa, T. (2012). Circuits for skilled reaching and grasping. Annu. Rev. Neurosci. 35, 559–578.
54. Fouad, K., Klusman, I., and Schwab, M.E. (2004). Regenerating corticospinal fibers in the Marmoset (Callitrix jacchus) after spinal cord lesion and treatment with the anti-Nogo-A antibody IN-1. Eur. J. Neurosci. 20, 2479–2482.
55. Freund, P., Schmidlin, E., Wannier, T., Bloch, J., Mir, A., Schwab, M.E., and Rouiller, E.M. (2006). Nogo-A-specific antibody treatment enhances sprouting and functional recovery after cervical lesion in adult primates. Nat. Med. 12, 790–792.
56. Freund, P., Wannier, T., Schmidlin, E., Bloch, J., Mir, A., Schwab, M.E., and Rouiller, E.M. (2007). Anti-Nogo-A antibody treatment enhances sprouting of corticospinal axons rostral to a unilateral cervical spinal cord lesion in adult macaque monkey. J. Comp. Neurol. 502, 644–659.
57. Inoue, T., Lin, A., Ma, X., McKenna, S.L., Creasey, G.H., Manley, G.T., Ferguson, A.R., Bresnahan, J.C., and Beattie, M.S. (2013). Combined SCI and TBI: recovery of forelimb function after unilateral cervical spinal cord injury (SCI) is retarded by contralateral traumatic brain injury (TBI), and ipsilateral TBI balances the effects of SCI on paw placement. Exp. Neurol. 248, 136–147.
58. Ringner, M. (2008). What is principal component analysis? Nat. Biotechnol. 26, 303-304.
59. Mahmood, N.S., Kadavigere, R., Avinash, K.R., and Rao, V.R. (2008). Magnetic resonance imaging in acute cervical spinal cord injury: a correlative study on spinal cord changes and 1 month motor recovery. Spinal Cord 46, 791–797.
60. Ramon, S., Dominguez, R., Ramirez, L., Paraira, M., Olona, M., Castello, T., and Garcia Fernandez, L. (1997). Clinical and magnetic resonance imaging correlation in acute spinal cord injury. Spinal Cord 35, 664–673.
61. Lammertse, D., Dungan, D., Dreisbach, J., Falci, S., Flanders, A., Marino, R., and Schwartz, E.; National Institute on Disability and Rehabilitation. (2007). Neuroimaging in traumatic spinal cord injury: an evidence-based review for clinical practice and research. J. Spinal Cord Med. 30, 205–214.
62. Denny-Brown, D., Kirk, E.J., and Yanagisawa, N. (1973). The tract of Lissauer in relation to sensory transmission in the dorsal horn of spinal cord in the macaque monkey. J. Comp. Neurol. 151, 175–200.
63. Brown-Sequard, C.E. (1849). De la transmission des impressions sensitives par la moelle epiniere. C. R. Soc. Biol. 1, 192–194.
64. Kalsi-Ryan, S., Beaton, D., Curt, A., Popovic, M.R., Verrier, M.C., and Fehlings, M.G. (2014). Outcome of the upper limb in cervical spinal cord injury: profiles of recovery and insights for clinical studies. J. Spinal Cord Med. 37, 503–510.
65. University of Alabama. (2014). National Spinal Cord Injury Statistical Center, Facts and Figures at a Glance. Available at: www.nscisc.uab.edu. Accessed November 21, 2015.
66. Lu, P., Wang, Y., Graham, L., McHale, K., Gao, M., Wu, D., Brock, J., Blesch, A., Rosenzweig, E.S., Havton, L.A., Zheng, B., Conner, J.M., Marsala, M., and Tuszynski, M.H. (2012). Long-distance growth and connectivity of neural stem cells after severe spinal cord injury. Cell 150, 1264–1273.

Address correspondence to:
Jacqueline C. Bresnahan, PhD or
Michael S. Beattie, PhD
Department of Neurological Surgery
University of California at San Francisco
1001 Potrero Avenue
San Francisco, CA 94103-0555

E-mail: jacqueline.bresnahan@ucsf.edu;
michael.beattie@ucsf.edu